AIP | The Journal of Chemical Physics

# Effect of dispersive long-range corrections to the pressure tensor: The vapour-liquid interfacial properties of the Lennard-Jones system revisited

F. J. Martínez-Ruiz, F. J. Blas, B. Mendiboure, and A. I. Moreno-Ventas Bravo

Citation: The Journal of Chemical Physics **141**, 184701 (2014); doi: 10.1063/1.4900773
View online: http://dx.doi.org/10.1063/1.4900773
View Table of Contents: http://scitation.aip.org/content/aip/journal/jcp/141/18?ver=pdfcov
Published by the AIP Publishing



# Effect of dispersive long-range corrections to the pressure tensor: The vapour-liquid interfacial properties of the Lennard-Jones system revisited

F. J. Martínez-Ruiz,[1,2] F. J. Blas,[1,2,a)] B. Mendiboure,[3] and A. I. Moreno-Ventas Bravo[2,4]
[1]*Departamento de Física Aplicada, Universidad de Huelva, 21071 Huelva, Spain*
[2]*Centro de Investigación de Física Teórica y Matemática, Universidad de Huelva, 21071 Huelva, Spain*
[3]*Laboratoire des Fluides Complexes et leurs Réservoirs, UMR5150, Université de Pau et des Pays de l'Adour, B. P. 1155, Pau Cedex 64014, France*
[4]*Departamento de Geología, Facultad de Ciencias Experimentales, Universidad de Huelva, 21071 Huelva, Spain*

(Received 4 June 2014; accepted 20 October 2014; published online 10 November 2014)

We propose an extension of the improved version of the inhomogeneous long-range corrections of Janeček [J. Phys. Chem. B **110**, 6264–6269 (2006)], presented recently by MacDowell and Blas [J. Chem. Phys. **131**, 074705 (2009)] to account for the intermolecular potential energy of spherical, rigid, and flexible molecular systems, to deal with the contributions to the microscopic components of the pressure tensor due to the dispersive long-range corrections. We have performed Monte Carlo simulations in the canonical ensemble to obtain the interfacial properties of spherical Lennard-Jones molecules with different cutoff distances, $r_c = 2.5$, 3, 4, and $5\sigma$. In addition, we have also considered cutoff distances $r_c = 2.5$ and $3\sigma$ in combination with the inhomogeneous long-range corrections proposed in this work. The normal and tangential microscopic components of the pressure tensor are obtained using the mechanical or virial route in combination with the recipe of Irving and Kirkwood, while the macroscopic components are calculated using the Volume Perturbation thermodynamic route proposed by de Miguel and Jackson [J. Chem. Phys. **125**, 164109 (2006)]. The vapour-liquid interfacial tension is evaluated using three different procedures, the Irving-Kirkwood method, the difference between the macroscopic components of the pressure tensor, and the Test-Area methodology. In addition to the pressure tensor and the surface tension, we also obtain density profiles, coexistence densities, vapour pressure, critical temperature and density, and interfacial thickness as functions of temperature, paying particular attention to the effect of the cutoff distance and the long-range corrections on these properties. According to our results, the main effect of increasing the cutoff distance (at fixed temperature) is to sharpen the vapour-liquid interface, to decrease the vapour pressure, and to increase the width of the biphasic coexistence region. As a result, the interfacial thickness decreases, the width of the tangential microscopic component of the pressure tensor profile increases, and the surface tension increases as the cutoff distance is larger. We have also checked the effect of the impulsive contribution to the pressure due to the discontinuity of the intermolecular interaction potential when it is cut. If this contribution is not accounted for in the calculation of the microscopic components of the pressure tensor, incorrect values of both components as well as a wrong structure along the vapour-liquid interface are obtained.  [http://dx.doi.org/10.1063/1.4900773]

## I. INTRODUCTION

The phenomenology associated to fluid-fluid interfacial properties has fascinated scientifics since the time of Laplace and Young.[1] The determination of interfacial properties, and particularly surface tension, has been always an ambitious and challenging goal for many computer simulation researchers of the liquid-state community. Understanding how different microscopic mechanisms determine the thermodynamic and structural behaviour of systems that exhibit a fluid-fluid interface is essential in a large number of scientific and engineering fields, including nucleation or dynamics of phase transition, among many others. However, the fluid-fluid surface tension is probably the most challenging property to be determined and predicting using molecular-based theories and simulation techniques. Despite the number of studies carried out since computer simulation is used routinely for determining the properties of a molecular model, the calculation of surface tension is still a subtle problem. The ambiguity in the definition of the microscopic components of the pressure tensor,[2,3] the finite size effects due to capillary waves,[4,5] or the difficulty for the calculation of the dispersive long-range corrections (LRC) associated to the intermolecular interactions,[6,7] make the calculation of surface tension a difficult and non-trivial problem.

The usual procedure to the evaluation of the fluid-fluid interfacial tension in a molecular simulation involves the

a)Electronic mail: felipe@uhu.es

 

determination of the microscopic components of the pressure tensor through the well-known mechanical or virial route. This route states that surface tension of a planar fluid-fluid interface can be readily obtained from the integration of the difference between the normal $P_N(z)$ and tangential $P_T(z)$ microscopic components of the pressure tensor profiles along the interface as

$$\gamma = \int_0^{L_z} \left( P_N(z) - P_T(z) \right) dz. \tag{1}$$

Note that here we have chosen the $z$-axis perpendicular to the interface and the integral is performed along the total length $L_z$ of the simulation box. Care must be taken in cases in which there exist two vapour-liquid interfaces, which is the standard procedure for studying direct fluid-fluid coexistence in Monte Carlo (MC) and Molecular Dynamics (MD) simulation. In this case, the true value associated to a single interface is half of the value obtained from Eq. (1).

This method generally involves an ensemble average of the virial of Clausius according to the recipes of Irving and Kirkwood[8] (IK) or Harasima,[9] among many others possible choices. Although the mechanical route is especially appropriate when molecular dynamics techniques are used to determine the interfacial tension of a system, since the evaluation of the forces is required to determine the molecular trajectories, a number of alternative methods have been proposed during the last years to calculate, not only the interfacial tension, but also for the components of the pressure tensor, without the need to evaluate the virial. The origin of these new techniques is probably due to the increasing capacity of computers for calculating larger and more complex systems and the interest of the condensed matter community for understanding from a molecular perspective the mechanisms that control the macroscopic behaviour of interfaces of fluids.

These alternative methods are especially suited in Monte Carlo simulations, in which the calculation of the forces is not required for sampling the configurational space of the system. In addition to that, although the evaluation of the virial is straightforward in systems interacting through simple intermolecular potentials, this is not the case for complex intermolecular interactions, including those governing the microscopic behaviour of chain-like molecules or system with specific interactions, and particularly models in which the intermolecular potential is discontinuous, such as the hard-sphere and square-well potentials, and in cases in which specific interactions are modeled as associating square-well sites, among others. In this situation, the evaluation of forces can be difficult and very time consuming. Exceptions to this rule in the literature are the works of Chapela, Alejandre and co-workers,[10–13] and Malfreyt and co-workers.[14,15]

The new generation of alternative methods for determining the surface tension and the components of the pressure tensor constitute a collection of effective and elegant techniques based on the thermodynamic definition of these properties. Consider a system in which the number of particles, $N$, the volume $V$, and temperature $T$ are constant. Under these conditions, the appropriate definition of surface tension $\gamma$ can be written as

$$\gamma = \left( \frac{\partial F}{\partial \mathcal{A}} \right)_{NVT}. \tag{2}$$

The surface tension can be understood as the change in free energy $F$ of the system for an infinitesimal change in the interfacial area, $\mathcal{A}$, while keeping $N$, $V$, and $T$ constant. Assuming the same conditions, the diagonal components of the pressure tensor of the system, $P_{\alpha\alpha}$, with $\alpha = x, y, z$, following de Miguel and Jackson,[16] can be expressed using its thermodynamic definition as

$$P_{\alpha\alpha} = -\left( \frac{\partial F}{\partial V} \right)_{NTL_{\beta\neq\alpha}}. \tag{3}$$

The notation $L_{\beta\neq\alpha}$ indicates that the partial derivative with respect to the volume is performed in such a way that the dimension of the system along the $\alpha$-axis, $L_\alpha$, is varied while keeping all other dimensions $L_\beta$ ($\beta \neq \alpha$) fixed.

Equations (2) and (3) allow two different interpretations for calculating the surface tension and the components of the pressure tensor. In the first approach, the one we focus on exclusively in this work, equations can be written using basic Statistical Mechanics as configurational averages over the unperturbed system of surface area $\mathcal{A}$ and volume $V$ of appropriate Boltzmann factors. These expressions (see Eq. (60) of the original work of Gloor *et al.*,[3] and Eqs. (8)–(9) and (16)–(17) of the work of de Miguel and Jackson[16] for further details) suggest that both magnitudes can be calculated averaging the corresponding Boltzmann factors associated with virtual changes of surface area and volume, respectively. This approach corresponds to perturbative approaches such as the Test-Area (TA) technique[3] for the surface tension and the Volume Perturbation (VP) methods for the determination of the macroscopic components of the pressure tensor.[16–18] These methods are becoming very popular and are being used routinely to determine the vapour-liquid interfacial properties of Lennard-Jones (LJ),[7,19–21] several models of water,[22,23] the Mie potential,[24] binary mixtures,[25–27] or real systems[15,28–33] among others.

Another interpretation for calculating the surface tension and the components of the pressure tensor using the thermodynamic definition of both magnitudes, given by Eqs. (2) and (3), is possible. In the former approach, they are evaluated averaging Boltzmann factors using virtual changes of the system, i.e., the perturbed states generated during the simulation do not correspond to real states sampled along the Markov chain generated during the simulation. Because of that most of these methods receive the generic name of perturbative methods. The second class of methods that exploit the use of Eqs. (2) and (3) are non-perturbative techniques, in which the interfacial area is sampled along the simulation, i.e., states with unperturbed and perturbed interfacial areas are explicitly considered in the Markov chain of the simulation. Representative examples of methods that follow this approach are the use of the Expanded Ensemble (EE), based on the original work of Lyuvartsev *et al.*,[34] for calculating the surface tension proposed independently by Errington and Kofke[35] and de Miguel,[36] and the Wandering Interface Method (WIM), introduced by MacDowell and Bryk.[37] In the first method,

states of the system are sampled through a global set of subensembles, with different interfacial areas, allowing to calculate the difference in free energy between states (basically, the surface tension) in terms of the probability of finding the system in these states.[35,36] The second methodology, the WIM technique, can be viewed as a continuous version of the EE method in which the interfacial area is allowed to fluctuate randomly and the surface tension can be obtained from the analysis of the resulting probability distribution. The WIM approach has been successfully used for determining the fluid-fluid and solid-fluid interfacial tension of a variety of complex systems.[7,19,38–40]

As mentioned previously, one of the major difficulties encountered in the simulation of inhomogeneous systems by molecular simulation is the truncation of the intermolecular potential. Although for homogeneous systems this issue is easily solved by including the well-known homogeneous LRC,[41,42] the situation is much more complicated in the case of fluid-fluid interfaces, and in general, in inhomogeneous systems. Fortunately, this problem seems to solved satisfactorily recently in cases in which the system exhibits planar symmetry. Different authors have contributed to the establishment of appropriate and standard inhomogeneous LRC, including Blokhius,[43] Mecke,[44,45] Daoulas,[46] Guo and Lu,[47] and finally, Janeček,[6,48] and the recent improved methods proposed by MacDowell and Blas[7] and de Gregorio *et al.*[39]

The truncation of the intermolecular potential has important effects on the calculation of any physical property. In general, all properties exhibit a dependence with the cutoff distance, but the relative effect is different depending on the specific magnitude. Though the density profiles, coexistence densities, and critical coordinates are affected by the truncation, the interfacial thickness and more particularly the surface tension show a stronger dependence on the particular choice of the cutoff distance.[6,7,19,49,50] The effect of truncation on the surface tension was already noted by the seminal work of Chapela *et al.*[51] and discussed very nicely by Trokhymchuk and Alejandre.[49] These latter authors also analyzed in detail the truncation procedure and the presence of an additional force due to the discontinuity of the truncated potential at the cutoff distance. This additional force due to the discontinuity of the truncated potential at cutoff distance becomes crucial for inhomogeneous fluids and has to be included into the virial calculation in both Monte Carlo and Molecular Dynamics, as well as into the computation for interactions in Molecular Dynamics simulations.

Although different authors have recently considered the effect of truncating and applying the appropriate LRC to systems that interact through the spherical LJ intermolecular potential[3,6,50] on the surface tension, the number of studies devoted to determine the effect of using different cutoff distances for the intermolecular potential on the components of the pressure tensor is really scarce.

The main goal of this work is twofold. First, we propose an improved version of the original LRC of Janeček,[6] based on a previous work of one of us to deal with the intermolecular potential energy,[7] to estimate the LRC associated to the microscopic components of the pressure tensor of a spherical model in a planar fluid-fluid interface. Second, we revisit the interfacial properties of the LJ spherical model, including the density profiles, interfacial thickness, surface tension, and normal and tangential microscopic and macroscopic components of the pressure tensor. We also determine other thermodynamic properties, such as coexistence densities, vapour pressure, and critical temperature and density. In particular, we consider the spherical truncated (but not shifted) intermolecular potential with different cutoff distances, from $r_c = 2.5$ up to $5\sigma$. We also pay special attention to the effect of neglecting the impulsive contribution to the components of the pressure tensor associated to the discontinuity of the potential at the cutoff distance $r_c$. In addition to that, we also consider the full intermolecular potential, i.e., the potential truncated at $r_c = 2.5$ and $3\sigma$ with the version of inhomogeneous LRC of MacDowell and Blas[7] based on the Janeček's work[6] for the potential energy and the improved version proposed in this work for the components of the pressure tensor. In order to assess the effectiveness of the new methodology proposed, we have also determined the surface tension and the components of the pressure tensor using two different perturbative methods, the TA technique and the VP methodology. This allows to obtain independent results and compare our predictions with simulation data taken from the literature.

The rest of the paper is organized as follows. In Sec. II, we consider an improved method for determining the contribution to the microscopic components of the pressure tensor due to the LRC of inhomogeneous spherical systems. The molecular model and the simulation details of this work are presented in Sec. III. Results obtained are discussed in Sec. IV. Finally, in Sec. V we present the main conclusions.

## II. EFFECTIVE LONG-RANGE PAIRWISE CORRECTIONS FOR THE PRESSURE TENSOR OF SPHERICAL SYSTEMS

In 2006, Janeček[6] proposed a new methodology for calculating LRC to the energy and pressure tensor in systems that interact through spherically symmetric intermolecular potentials. This procedure allows to treat in a simple way the truncation of the intermolecular energy of systems that exhibit planar interfaces. More recently, MacDowell and Blas[7] have demonstrated that the Janeček's procedure can be rewritten into an effective long-range pair potential plus a self term that allows for a fast, easy, and elegant implementation of the method. In this work, we extend this improved version to deal with the long-range pair potential contributions to the components of the pressure tensor. Since the original methodology has been introduced elsewhere,[6,48,52,53] the most important details corresponding to the LRC term to the components of the pressure tensor proposed by Janeček[6] are provided in the supplementary material.[54] Here, we focus the attention to the extension of the improved version for dealing with the pressure tensor.

As mentioned previously, MacDowell and Blas[7] have proposed an improved methodology of the Janeček's[6] method for dealing with the intermolecular interactions of an inhomogeneous system due to LRC. The method, which is simpler and more accurate, elegant, and easier to implement in a simulation code than the original one, has been applied

successfully to calculate the interfacial properties of several models, including fully flexible and rigid-linear Lennard-Jones chains[7,55–57] and water and carbon dioxide.[58] Following the recipe of MacDowell and Blas,[7,58] Eq. (10) of the supplementary material[54] is written more accurately as

$$\Pi^{\mathrm{LRC}}_{\alpha\alpha}(z_i) = \left\langle \int_{-\infty}^{+\infty} \pi_{\alpha\alpha}(|z_i - z|)\, \rho(z)\, dz \right\rangle. \tag{4}$$

The density profile of a system formed by $N$ particles can be written formally as a summation of $\delta$-Dirac distributions centered at the positions $z_j$, with $j = 1, \ldots, N$,

$$\rho(z) = \frac{1}{\mathcal{A}} \sum_{j=1}^{N} \delta(z - z_j), \tag{5}$$

where $\mathcal{A}$ is the interfacial area of the $xy$-plane of the system. Using Eq. (5) in Eq. (4), $\Pi^{\mathrm{LRC}}_{\alpha\alpha}(z_i)$ is given by

$$\Pi^{\mathrm{LRC}}_{\alpha\alpha}(z_i) = \left\langle \frac{1}{\mathcal{A}} \sum_{j=1}^{N} \pi_{\alpha\alpha}(|z_i - z_j|) \right\rangle. \tag{6}$$

It is important to note that summation in Eq. (6) runs over all the values of the index $j$ ($j = 1, \ldots, N$), and this also included the case $j = i$.

The total components of the virial tensor arising from the LRC, defined by Eq. (9) of the supplementary material,[54] is then expressed as

$$\Pi^{\mathrm{LRC}}_{\alpha\alpha} = \frac{1}{2} \sum_{i=1}^{N} \Pi^{\mathrm{LRC}}_{\alpha\alpha}(z_i) = \left\langle \frac{1}{2\mathcal{A}} \sum_{i=1}^{N} \sum_{j=1}^{N} \pi_{\alpha\alpha}(|z_i - z_j|) \right\rangle. \tag{7}$$

The unrestricted summation over indexes $i$ and $j$ can be finally transformed into a sum of pairwise effective (integrated) intermolecular virial over all the pairs of molecules in the system and $N$ self-energy terms as

$$\begin{aligned} \Pi^{\mathrm{LRC}}_{\alpha\alpha} &= \left\langle \frac{1}{\mathcal{A}} \sum_{i=1}^{N-1} \sum_{j=i+1}^{N} \pi_{\alpha\alpha}(|z_i - z_j|) \right\rangle + \left\langle \frac{1}{2\mathcal{A}} \sum_{i=1}^{N} \pi_{\alpha\alpha}(0) \right\rangle \\ &= \left\langle \frac{1}{\mathcal{A}} \sum_{i=1}^{N-1} \sum_{j=i+1}^{N} \pi_{\alpha\alpha}(|z_i - z_j|) \right\rangle + \left\langle \frac{N}{2\mathcal{A}} \pi_{\alpha\alpha}(0) \right\rangle. \end{aligned} \tag{8}$$

The expressions given by Eqs. (6) and (8) are the key relationships that generalize the improved version proposed by MacDowell and Blas[7] for dealing with the components of the pressure tensor: the components of the pressure tensor due to the LRC are given by an effective pairwise components pressure tensor between all the particles forming the system.

The last term in Eq. (8), the self-tensor contribution, is not a truly summation of self-virial tensor terms. In fact, the function $\pi_{\alpha\alpha}(z)$ is not a real contribution to the component of the virial tensor between a pair of particles but an effective (integrated) component of the virial tensor. Each contribution $\frac{1}{\mathcal{A}}\pi_{\alpha\alpha}(|z_i - z_j|)$ in Eq. (6) represents the contribution to the component of the virial tensor, due to the interactions between the particle $i$ with all the particles located inside the slab centered at $z_j$ due to the long-range interactions. Therefore, $\pi_{\alpha\alpha}(0)$ represents the contribution to the component of the virial tensor due to the interactions between a molecule and the rest of molecules located inside the same slab but beyond the cut-off radius.

This procedure provides several important advantages over the original method: (1) Eqs. (6) and (8) correspond to the exact evaluation of the components of the virial tensor due to the LRC. It is important to recall that the use of the original Janeček version of the method implies a discretization of the simulation box along the $z$-axis, which is in fact an approximation; (2) the improved procedure allows to evaluate $\Pi^{\mathrm{LRC}}_{\alpha\alpha}(z_i)$ and $\Pi^{\mathrm{LRC}}_{\alpha\alpha}$ without the explicit calculation of the density profile on the fly, i.e., it is not necessary to update the density profile $\rho(z)$ each Monte Carlo step, and consequently, to perform the double integral shown in the original work of Janeček (see Eq. (23) of the original paper[6]).

## III. MODEL AND SIMULATION DETAILS

We consider spherical LJ molecules characterized by a diameter $\sigma$ and dispersive energy $\epsilon$. The interaction potential between two different molecules is given by

$$u_{LJ}(r) = 4\epsilon \left[ \left(\frac{\sigma}{r}\right)^{12} - \left(\frac{\sigma}{r}\right)^{6} \right], \tag{9}$$

where $r$ is the distance between two molecules. During the simulation, we use a potential spherically truncated (but not shifted) at a cutoff distance $r_c$, defined by

$$u(r) = u_{LJ}(r)\left[1 - \Theta(r - r_c)\right] = \begin{cases} u_{LJ}(r) & r \le r_c \\ 0 & r > r_c \end{cases}, \tag{10}$$

where $\Theta(x)$ is the Heaviside step function.

We examine this spherically truncated potential model with several cutoff distances, $r_c = 2.5$, 3, 4, and $5\sigma$. In addition to that, we study the interfacial and thermodynamic properties of spherically truncated LJ potential with $r_c = 2.5$ and $3\sigma$ considering inhomogeneous LRC using the MacDowell and Blas[7,56] methodology for the intermolecular potential energy and the recipe presented in Sec. II, based on the Janeček's method,[6,48] for the evaluation of the LRC for the components of the pressure tensor. Results obtained using these LRC are equivalent to use the full potential or a potential with infinite truncation distance.

The number of molecules, $N$, used in all the simulations performed in this work is constant, $N = 2048$. As in previous studies,[7,19,39,55–59] this choice is made so as to have systems with the same total number of molecules. Simulations are performed in the $NVT$ ensemble. We consider a system of $N$ molecules at a temperature $T$ in a volume $V = L_x L_y L_z$, where $L_x$, $L_y$, and $L_z$ are the dimensions of the rectangular simulation box. A homogeneous liquid system is first equilibrated in a rectangular simulation box of dimensions $L_x = L_y = 12\sigma$, and $L_z = 16.891\sigma$ for the lowest temperature considered ($T^* = k_B T/\epsilon = 0.70$), and $L_z = 21.153\sigma$ for the highest temperature ($T^* = 1.1$). The box is then expanded to three times its original size along the $z$ direction, while leaving the liquid phase at the center with empty boxes of equal size at each side. The final overall dimensions of the vapour-liquid-vapour simulation box are therefore $L_x = L_y = 12\sigma$, and $L_z = 50.673\sigma$ for the lowest temperature considered

($T^* = 0.70$), and $L_z = 66.460\sigma$ for the highest temperature ($T^* = 1.1$).

The simulations are organized in cycles. A cycle is defined as $N$ trial moves (displacement of the center of mass) and the magnitude of the appropriate displacement is adjusted so as to get an acceptance rate of 30% approximately. We use periodic boundary conditions and minimum image convention in all three directions of the simulation box.

We have obtained the normal and tangential microscopic components of the pressure tensor from the mechanical expression or virial route. In particular, we have used the well-known IK recipe for determining the microscopic components of the pressure tensor, $P_N(z) \equiv P_{zz}(z)$ and $P_T(z) \equiv P_{xx}(z) \equiv P_{yy}(z) \equiv \frac{1}{2}(P_{xx}(z) + P_{yy}(z))$.[8] As explained in Sec. II, the simulation box is divided into slabs of width $\Delta z$ and area $\mathcal{A}$ parallel to the interface ($xy$-plane). The contribution to the microscopic pressure tensor at each point of the simulation box, due to a pair of molecules $i$ and $j$ located at $z_i$ and $z_j$, respectively, is obtained from the distribution of the pair virial among all slabs between $z_i$ and $z_j$ for both the normal and tangential components. Note that this also includes the contribution due to the LRC. In the improved version introduced in this work, based on the previous work of MacDowell and Blas,[7,56] the contribution due to the LRC are written as an effective pairwise components of the pressure tensor between all the molecules, resulting an elegant and effective way of accounting for this contribution. In practice, to determine the contribution to the pressure due to a given pair of molecules we perform the following steps:

1. We evaluate the distance along the $z$-axis between the pair of molecules $i$ and $j$, $|z_{ij}|$. To be consistent with the calculation of the intermolecular interactions performed during the simulation, the minimum image convention is also used when this contribution is calculated.
2. We then calculate the number of slabs between molecules $i$ and $j$ (after the minimum image convention is applied), including the slabs occupied by the molecules.
3. The contribution arising from the interactions between particles $i$ and $j$, including the contribution due to LRC, is divided by the number of slabs obtained in point 2.
4. Finally, the pressure contribution obtained in point 3 is then assigned equally to each slab between positions $z_i$ and $z_j$, including the slabs corresponding to positions $z_i$ and $z_j$ at which the molecules are located.

Since we are dealing with pairwise interactions, the total contribution to the components of the pressure tensor is obtained taking into account all the molecular pairs and averaging the total virial over the canonical ensemble. The final expression of the microscopic components of the pressure tensor are given by

$$P_N(z) = \langle \rho(z)\, k_B T \rangle + P_N^{\mathrm{CUT}}(z) + P_N^{\mathrm{LRC}}(z). \tag{11}$$

The first term of the right-hand side of Eq. (11) corresponds to the ideal (kinetic) contribution to the microscopic pressure tensor. Note that this contribution is obtained from the value of the density profile at the same position $z$. The two other terms, $P_N^{\mathrm{CUT}}(z)$ and $P_N^{\mathrm{LRC}}(z)$, are the contributions to the normal microscopic component of the pressure tensor, $P_N(z)$, due to the direct interactions between molecular pairs and LRC, respectively. A similar expression is also valid for the tangential microscopic component $P_T(z)$.

The contribution to normal component of the pressure tensor due to the direct interactions between molecular pairs, $P_N^{\mathrm{CUT}}(z)$, can be written as

$$\begin{aligned} P_N^{\mathrm{CUT}}(z) &= -\frac{1}{\mathcal{A}} \left\langle \sum_{i=1}^{N-1} \sum_{j=i+1}^{N} \frac{z_{ij}^2}{r_{ij}} \frac{\mathrm{d}u_{LJ}(r_{ij})}{\mathrm{d}r_{ij}} \frac{1}{|z_{ij}|} \right. \\ &\quad \left. \times \Theta\left(\frac{z - z_j}{z_{ij}}\right) \Theta\left(\frac{z_j - z}{z_{ij}}\right) \right\rangle \\ &= -\frac{1}{\mathcal{A}\,\Delta z} \left\langle \sum_{i=1}^{N-1} \sum_{j=i+1}^{N} \frac{z_{ij}^2}{r_{ij}} \frac{\mathrm{d}u_{LJ}(r_{ij})}{\mathrm{d}r_{ij}} \frac{1}{n_{ij}} \right\rangle. \end{aligned} \tag{12}$$

The corresponding contribution to the tangential component, $P_T^{\mathrm{CUT}}(z)$, is given by an expression of the form of Eq. (12) but with $(x_{ij}^2 + y_{ij}^2)/2$ instead of $z_{ij}^2$. Here, the factor $1/n_{ij}\Delta z$, proportional to the product of $1/|z_{ij}|$ and the two Heaviside step functions, is used to select the position at which the interaction between particles $i$ and $j$ contributes to the pressure tensor. In practice, if particles $i$ and $j$ are located at slabs $k_i$ and $k_j$, respectively, the number of the slabs located between them is $n_{ij} = |k_j - k_i| - 1$.

Using Eqs. (7) and (9) of the supplementary material,[54] Eq. (8), and taking into account the recipe of Irving and Kirkwood,[8] the contribution to the normal component of the pressure tensor due to LRC, $P_N^{\mathrm{LRC}}(z)$, can be written as

$$\begin{aligned} P_N^{\mathrm{LRC}}(z) &= \frac{1}{\mathcal{A}\,\Delta z} \left\{ \left\langle \frac{1}{\mathcal{A}} \sum_{i=1}^{N-1} \sum_{j=i+1}^{N} \pi_{zz}(|z_i - z_j|) \frac{1}{n_{ij}} \right\rangle \right. \\ &\quad \left. + \left\langle \frac{1}{2\mathcal{A}} \pi_{zz}(0) \right\rangle \right\}. \end{aligned} \tag{13}$$

The corresponding contribution to the tangential component, $P_T^{\mathrm{LRC}}(z)$, is given by an expression of the form of Eq. (13) but using $(\pi_{xx} + \pi_{yy})/2$ instead of $\pi_{zz}$. Here, $\pi_{\alpha\alpha}(|z_i - z_j|)$, with $\alpha = x, y, z$, are the same functions defined previously by Eqs. (11) and (12) of supplementary material.[54] Note that function $w(z, z_i, z_j)$ is also used in Eq. (13). This means that the pressure due to the LRC associated to the virial of particles at $z_i$ and $z_j$ contributes to all the slabs located between them (including the slabs at positions $z_i$ and $z_j$). The last term of the right-hand side of Eq. (13) represents the contribution to the pressure, due to the LRC, associated to the interaction between a particle and all the molecules located at the same slab. According to the meaning of this self-tensor contribution, as discussed previously in Sec. II, and to be consistent with the Irving-Kirkwood recipe for the calculation of the microscopic components of the pressure tensor, this term contributes to the pressure at position at which each particle is located in the simulation box.

We have also determined the macroscopic components of the pressure tensor using virtual volume perturbations of magnitude $\xi = \Delta V/V$ each cycle. Here, $\xi$ defines the relative volume (compressive and expansive) change

associated with the perturbation. We follow the methodology proposed by de Miguel and Jackson,[16] based on the seminal works of Eppenga and Frenkel[60] and Harismiadis *et al.*,[61] and rescale independently the box lengths of the simulation cell and positions of the molecular centers of mass according to linear transformations. In particular, the macroscopic average of the normal component of the pressure $P_N$ is computed (see Eq. (60) of the original work of Gloor *et al.*,[3] and Eqs. (16) and (17) of the work of de Miguel and Jackson[16]) by averaging the corresponding Boltzmann factor associated with a volume perturbation in which the normal dimension of the simulation cell is changed according to the transformation $L_z' = (1+\xi)L_z$ (including compression and expansion changes applied independently) while the transverse dimension remains unchanged. The macroscopic average of the tangential component $P_T$ is calculated from the same equations by considering a perturbation in which the tangential dimension of the system is changed isotropically according to $L_\alpha' = (1+\xi)^{1/2}L_\alpha$, with $\alpha = x, y$ (including compression and expansion changes applied independently), keeping $L_z$ fixed. In both cases, eight different (positive and negative) relative volume changes in the range $2 \times 10^{-4} \leq |\xi| \leq 15 \times 10^{-4}$ are used in our calculations. The final values of the macroscopic components of the pressure tensors presented in this work, $P_N$ and $P_T$, correspond to the extrapolated values (as determined by a linear extrapolation to $|\xi| \to 0$ of the values obtained from increasing-volume and decreasing-volume perturbations) obtained from a combined compression-expansion perturbation.

Finally, we have also calculated the surface tension using of the TA methodology.[3] Since the method is a standard and well-known procedure for evaluating fluid-fluid interfacial tensions of molecular systems, here we only provide the most important features of the technique. For further details, we recommend the original work[3] and the most important applications.[7,16,19,22–27,30,31,39,55–59] The implementation of the TA technique involves performing virtual or test area deformations of relative area changes defined as $\xi = \Delta\mathcal{A}/\mathcal{A}$ during the course of the simulation at constant $N$, $V$, and $T$ every MC cycle. As shown by Gloor *et al.*,[3] the surface tension follows from the computation of the change in Helmholtz free energy associated with the perturbation, which in turn can be expressed as an ensemble average of the corresponding Boltzmann factor. Further details can be found in Ref. 3. Note that the procedure for calculating the surface tension is similar to that used to evaluate the components of the pressure tensor, but in this case the changes in the normal and transverse dimensions are coupled to keep the overall volume constant. In particular, we use the same number and values for the relative area changes $\xi$, and the same procedure to obtain the extrapolated values.

As in previous studies,[7,19,39,55–59] for each cutoff distance (with and without LRC) we perform simulations of inhomogeneous systems at different temperatures where vapour-liquid equilibrium is expected. We typically consider seven temperatures in the range $\sim 0.5\,T_c$ up to $\sim 0.9\,T_c$, where $T_c$ is the critical temperature of the system. Each simulation box is well equilibrated for $10^6$ MC cycles, and averages are determined over a further period of $2 \times 10^6$ MC cycles. The production stage is divided into $M$ blocks. Normally, each block is equal to $10^5$ MC cycles. The ensemble average of the macroscopic components of the pressure tensor and the surface tension is given by the arithmetic mean of the block averages and the statistical precision of the sample average is estimated from the standard deviation in the ensemble average from $\overline{\sigma}/\sqrt{M}$, where $\overline{\sigma}$ is the variance of the block averages, and $M = 20$ in all cases.

All the quantities in our paper are expressed in conventional reduced units, with $\sigma$ and $\epsilon$ being the length and energy scaling units, respectively. Thus, the temperature is given in units of $\epsilon/k_B$, the densities in units of $\sigma^{-3}$, the pressure in units of the $\epsilon/\sigma^3$, the surface tension in units of $\epsilon/\sigma^2$, and the cutoff distance and interfacial thickness in units of $\sigma$.

## IV. RESULTS AND DISCUSSION

In this section, we present the main results from simulations of the vapour-liquid interface of spherical LJ molecules using different cutoff distances, with and without LRC for the intermolecular potential energy and components of the pressure tensor. We focus mainly on the effect of using different cutoff distances on the microscopic components of the pressure tensor. To our knowledge, little work has been devoted to study the effect of cutoff distance and LRC on the microscopic components of the pressure tensor.

We have determined the components of the pressure using both the mechanical (or virial) and thermodynamic routes. Comparison between both results allows to check the validity of the method presented in Sec. II for determining the contribution to the pressure due to the LRC. We have also examined several coexistence properties, such as coexistence densities and vapour pressures, and also other interfacial properties, such as density profiles, interfacial thickness, and surface tension. In particular, we pay special attention on the determination of the vapour-liquid interfacial tension calculated using different routes, including the mechanical or virial route (using the traditional IK methodology) and the thermodynamic definition (using the VP and TA methods) of the surface tension.

### A. Effect of cutoff distance and LRC on normal and tangential pressure

We first analyze the equilibrium normal and tangential components of the microscopic pressure tensor profiles, $P_N(z)$ and $P_T(z)$, respectively, that are computed from averages of histograms of pressures along the $z$ direction over the production stage, according to the IK prescription explained in Sec. III. As in the case of all properties calculated in this work, this procedure is meaningful as far as the central liquid slab is thick enough. This turns out to be the case in our simulations, including those performed at higher temperatures.

We consider the normal and tangential components of the microscopic pressure tensor profiles at a low temperature, $T = 0.72$. Fig. 1 shows $P_N(z)$ and $P_T(z)$ for spherical molecules with different cutoff distances for the intermolecular potential, from $r_c = 2.5$ up to 5. We have also included the results corresponding to a LJ cutoff distance $r_c = 3$ and the

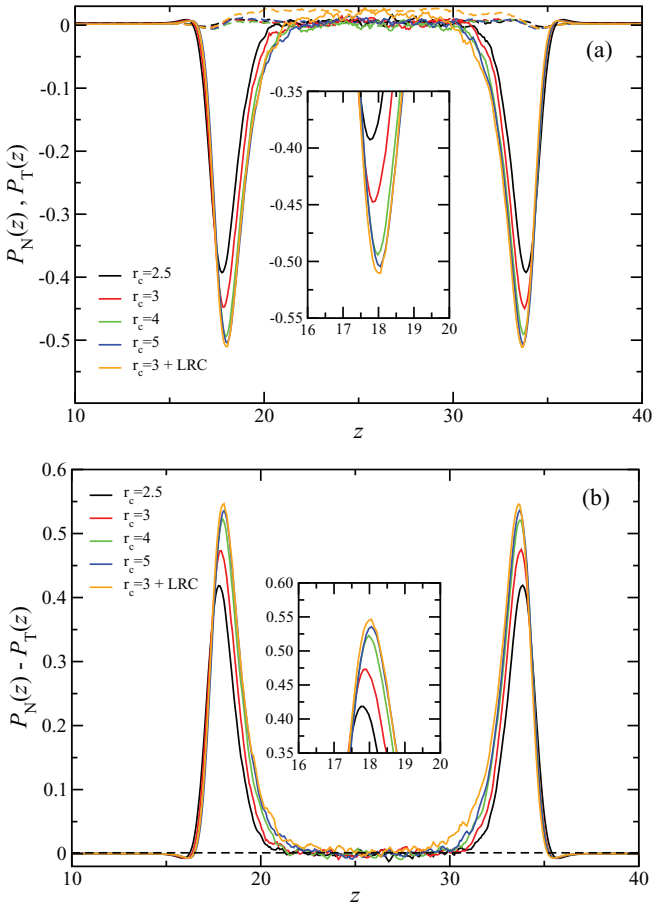


FIG. 1. Normal $P_N(z)$ and tangential $P_T(z)$ (a), and difference between the normal and tangential microscopic components (b) of the pressure tensor profiles across the two vapour-liquid interfaces of spherical LJ molecules at $T = 0.72$ and using cutoff distances $r_c = 2.5$ (black), 3 (red), 4 (green), 5 (blue), and 3 with inhomogeneous LRC (orange). Continuous and dashed curves in part (a) correspond to the tangential and normal microscopic components of the pressure tensor, respectively. Insets correspond to the enlargement of the interfacial region for $P_T(z)$ (a) and $P_N(z) - P_T(z)$ (b).

inhomogeneous LRC introduced in Sec. II (full LJ potential). Note that in all sections, except Subsection IV B (Effect of the impulsive contribution of the intermolecular force on pressure tensor), we have taken into account the impulsive contribution to the pressure due to the discontinuity of the intermolecular force at $r = r_c$. In particular, we follow the seminal work of Trokhymchuk and Alejandre.[49] See Subsection IV B for further details. Tables I and II show the values for the normal and tangential macroscopic components of the pressure tensor at different temperatures and cutoff distances. As can be seen in Fig. 1(a), the components of the microscopic pressure tensor along the two vapour-liquid interfaces exhibit the expected behaviour, i.e., the normal component of the pressure tensor profile is constant (within the statistical error) through the interface and equal to the vapour pressure of the system (according to the mechanical stability, that it requires the gradient of pressure tensor vanishes). In addition, the tangential component of the pressure tensor profile is approximately constant and equal to the normal pressure in the liquid and both vapour bulk-like regions of the simulation box. $P_T(z)$ becomes negative at the two interfacial regions of the system showing two (negative) local minima.

The values of $P_N(z)$ and $P_T(z)$ along the vapour slab are nearly independent of the cutoff distance used, including the values corresponding to the full potential. This is expected since vapour density is very low, especially at this temperature ($T = 0.72$), and contributions to the pressure due to particles separated beyond the lowest cutoff distance ($r_c = 2.5$) are negligible. A similar behaviour is also observed in the liquid slab, although the statistical noise is larger, as expected. However, the most interesting effect of the cutoff distance over the pressure tensor at this temperature is undeniably associated with the values of the two minima of $P_T(z)$. As can be seen, the cutoff distance has an enormous effect on this magnitude as its value is increased. In particular, the two minima values of $P_T(z)$ are a 23% higher than those corresponding to the values of the full potential for a cutoff distance of $r_c = 2.5$. Note that this difference is very important since, as it is well-known, are directly related with the value of the vapour-liquid surface tension of the system.

We have also calculated the difference of both components of the pressure tensor profile, as a function of the position along the $z$ direction. As can be seen in Fig. 1(b), the difference $P_N(z) - P_T(z)$ exhibits the expected shape, i.e., constant and equal to zero in the vapour and liquid slabs, since bulk-like regions do not contribute to the surface tension of the system, and positive peaks at both interfacial regions where the components of the pressure tensor are different due to the extra contribution of the tension to the tangential pressure at the interface. Differences between the maximum value reached by $P_N(z) - P_T(z)$ using a cutoff distance $r_c$ (without LRC) and the full potential decrease as the cutoff is increased, as expected.

We now consider the normal and tangential microscopic components of the pressure tensor, at a higher temperature, using the same cutoff distances for the LJ intermolecular potential and a cutoff distance $r_c = 3$ for the full LJ potential. The microscopic components of the pressure tensor, at $T = 1.0$, along the two vapour-liquid interfaces are shown in Fig. 2(a). As can be seen, both components exhibit the same qualitative behaviour as at low temperature ($T = 0.72$). The separation between both interfacial regions is now smaller than in the case corresponding to low temperatures due to the growth of the interfacial regions. The normal component of the pressure (which is equal to the vapour pressure of the system) decreases as the cutoff distance is increased. This effect, that is more noticeable than in Fig. 1(a) due to the scale employed now, is in fact larger than at low temperatures. See Table I for further details.

A similar behaviour is also observed in the case of the tangential microscopic component of the pressure tensor. The two minima values of $P_T(z)$ are higher than those corresponding to the values got for the full intermolecular potential when the cutoff distance $r_c$ is increased. These differences are systematically larger than those found at lower temperatures, as can be seen comparing Figs. 1(a) and 2(a).

Another interesting feature exhibited by the tangential microscopic component of the pressure tensor profiles, which is more evident at high temperatures, is the increase of the region of the interface at which $P_T(z) \neq P_N$ as the cutoff distance of the intermolecular potential is increased. These

TABLE I. Liquid density, $\rho_L$, vapour density, $\rho_V$, normal macroscopic component of the pressure tensor calculated from the virial route, $P_N^{\text{vir}}$, normal and tangential macroscopic components of the pressure tensor calculated from VP, $P_N^{VP}$ and $P_T^{VP}$, respectively, surface tension calculated from integration given by Eq. (1), $\gamma^{vir}$, from VP, $\gamma^{VP}$, and from TA, $\gamma_{TA}$, and 10–90 interfacial thickness, $t$ for a system of LJ molecules at different temperatures and cutoffs distances. All quantities are expressed in the reduced units defined in Sec. III. The errors are estimated as explained in the text. Uncertainties of surface tension calculated from the virial route, $\gamma^{vir}$, are error estimates corresponding to the numerical calculation of the integral given by Eq. (1).

| $r_c$ | $\rho_L$ | $\rho_V$ | $P_N^{vir}$ | $P_N^{VP}$ | $P_T^{VP}$ | $\gamma^{vir}$ | $\gamma^{VP}$ | $\gamma_{TA}$ | $t$ |
|---|---|---|---|---|---|---|---|---|---|
| | | | | $T = 0.70$ | | | | | |
| 2.5 | 0.8161(13) | 0.0035(3) | 0.00240(3) | 0.0028(7) | −0.0286(7) | 0.793(6) | 0.794(6) | 0.795(3) | 1.838(6) |
| 3 | 0.8283(14) | 0.00315(21) | 0.002138(17) | 0.0015(9) | −0.0340(9) | 0.902(10) | 0.901(7) | 0.903(3) | 1.794(2) |
| 4 | 0.8367(17) | 0.00246(18) | 0.001677(16) | 0.0023(6) | −0.0376(6) | 1.017(7) | 1.011(5) | 1.016(3) | 1.760(2) |
| 5 | 0.8394(23) | 0.0021(2) | 0.001398(12) | 0.0021(7) | −0.0403(7) | 1.072(9) | 1.073(6) | 1.074(5) | 1.7526(9) |
| | | | | $T = 0.72$ | | | | | |
| 2.5 | 0.8066(11) | 0.0048(3) | 0.00330(2) | 0.0031(7) | −0.0257(7) | 0.744(7) | 0.744(6) | 0.746(2) | 1.9054(18) |
| 3 | 0.8195(9) | 0.0038(3) | 0.00264(2) | 0.0032(7) | −0.0167(7) | 0.866(11) | 0.515(6) | 0.866(4) | 1.8652(4) |
| 4 | 0.8279(13) | 0.00305(19) | 0.002130(18) | 0.0018(7) | −0.0360(7) | 0.975(6) | 0.975(6) | 0.974(3) | 1.833(3) |
| 5 | 0.830(2) | 0.00296(19) | 0.002067(18) | 0.0030(10) | −0.0368(9) | 1.028(6) | 1.029(8) | 1.030(3) | 1.882(3) |
| | | | | $T = 0.80$ | | | | | |
| 2.5 | 0.7682(12) | 0.01007(23) | 0.007465(22) | 0.0076(7) | −0.0147(7) | 0.596(5) | 0.594(6) | 0.595(3) | 2.260(8) |
| 3 | 0.7829(11) | 0.0081(6) | 0.00610(5) | 0.0088(6) | −0.0173(6) | 0.697(10) | 0.696(5) | 0.698(4) | 2.1993(17) |
| 4 | 0.7915(13) | 0.00709(23) | 0.00536(3) | 0.0048(7) | −0.0255(8) | 0.809(15) | 0.809(6) | 0.810(3) | 2.147(7) |
| 5 | 0.7949(13) | 0.0070(4) | 0.00527(3) | 0.0045(8) | −0.0277(8) | 0.859(6) | 0.859(7) | 0.856(3) | 2.133(8) |
| | | | | $T = 0.90$ | | | | | |
| 2.5 | 0.7152(7) | 0.0265(9) | 0.02013(11) | 0.0198(8) | 0.0054(8) | 0.409(6) | 0.409(7) | 0.411(3) | 2.865(22) |
| 3 | 0.7302(11) | 0.0207(6) | 0.01632(7) | 0.0145(7) | −0.0031(6) | 0.498(10) | 0.497(6) | 0.497(3) | 2.733(5) |
| 4 | 0.7440(12) | 0.01690(6) | 0.01359(7) | 0.0142(8) | −0.0069(8) | 0.596(6) | 0.597(7) | 0.596(3) | 2.643(6) |
| 5 | 0.7470(21) | 0.0168(7) | 0.01308(7) | 0.0118(6) | −0.0107(7) | 0.635(7) | 0.636(6) | 0.635(2) | 2.633(3) |
| | | | | $T = 0.92$ | | | | | |
| 2.5 | 0.7041(8) | 0.0302(8) | 0.02311(8) | 0.0233(8) | 0.0100(8) | 0.382(5) | 0.381(7) | 0.380(3) | 3.014(7) |
| 3 | 0.7207(11) | 0.0235(7) | 0.01869(7) | 0.0196(7) | 0.0032(8) | 0.471(9) | 0.470(7) | 0.470(2) | 2.865(20) |
| 4 | 0.7325(9) | 0.0198(12) | 0.01603(13) | 0.0144(6) | −0.0050(6) | 0.558(6) | 0.557(6) | 0.557(2) | 2.750(9) |
| 5 | 0.7371(13) | 0.0181(6) | 0.01480(5) | 0.0142(6) | −0.0070(6) | 0.606(7) | 0.607(6) | 0.608(3) | 2.730(13) |
| | | | | $T = 1.00$ | | | | | |
| 2.5 | 0.6510(6) | 0.0528(13) | 0.03979(9) | 0.0385(7) | 0.0306(7) | 0.239(5) | 0.239(7) | 0.240(2) | 3.858(14) |
| 3 | 0.6738(10) | 0.0404(8) | 0.03241(7) | 0.0333(6) | 0.0226(5) | 0.327(8) | 0.327(5) | 0.327(2) | 3.528(10) |
| 4 | 0.6900(12) | 0.0341(6) | 0.02817(6) | 0.0280(5) | 0.0145(5) | 0.410(7) | 0.409(5) | 0.409(2) | 3.369(9) |
| 5 | 0.6954(14) | 0.0315(10) | 0.02627(6) | 0.0268(6) | 0.0120(6) | 0.449(5) | 0.450(6) | 0.4503(21) | 3.316(10) |
| | | | | $T = 1.10$ | | | | | |
| 2.5 | 0.5645(7) | 0.0959(20) | 0.06832(17) | 0.0688(4) | 0.0658(4) | 0.099(5) | 0.099(5) | 0.0998(22) | 5.793(14) |
| 3 | 0.6015(10) | 0.0759(23) | 0.05825(12) | 0.0588(4) | 0.0538(4) | 0.168(7) | 0.167(4) | 0.1674(19) | 4.99(6) |
| 4 | 0.6257(11) | 0.0614(10) | 0.05012(12) | 0.0504(4) | 0.0435(3) | 0.238(5) | 0.228(4) | 0.237(2) | 4.528(23) |
| 5 | 0.6330(13) | 0.0584(16) | 0.04818(16) | 0.0483(5) | 0.0403(4) | 0.268(5) | 0.268(5) | 0.269(2) | 4.460(19) |

TABLE II. Liquid density, $\rho_L$, vapour density, $\rho_V$, normal component of the macroscopic pressure tensor calculated from the virial route $P_N^{\text{vir}}$, normal and tangential components of the macroscopic pressure tensor calculated from VP, $P_N^{VP}$ and $P_T^{VP}$, surface tension calculated from integration given by Eq. (1), $\gamma^{vir}$, from VP, $\gamma^{VP}$, and from TA, $\gamma_{TA}$, and 10–90 interfacial thickness, $t$, at different temperatures for systems of LJ molecules with a cutoff distance $r_c = 3$ with inhomogeneous LRC. All quantities are expressed in the reduced units defined in Sec. III. The errors are estimated as explained in the text. Uncertainties of surface tension calculated from the virial route, $\gamma^{vir}$, are error estimates corresponding to the numerical calculation of the integral given by Eq. (1).

| $T$ | $\rho_L$ | $\rho_V$ | $P_N^{vir}$ | $P_N^{VP}$ | $P_T^{VP}$ | $\gamma^{vir}$ | $\gamma^{VP}$ | $\gamma_{TA}$ | $t$ |
|---|---|---|---|---|---|---|---|---|---|
| 0.70 | 0.8421(21) | 0.0020(2) | 0.001353(15) | 0.0002(7) | −0.0456(7) | 1.158(11) | 1.164(6) | 1.164(4) | 1.722(3) |
| 0.72 | 0.8338(22) | 0.00255(19) | 0.001779(15) | 0.0017(8) | −0.0414(8) | 1.110(10) | 1.114(6) | 1.116(4) | 1.824(3) |
| 0.80 | 0.7986(16) | 0.0063(2) | 0.00478(3) | 0.0048(7) | −0.0300(8) | 0.923(10) | 0.930(7) | 0.927(4) | 2.121(3) |
| 0.90 | 0.7517(13) | 0.0152(5) | 0.01234(6) | 0.0122(8) | −0.0130(7) | 0.712(9) | 0.713(7) | 0.713(3) | 2.601(16) |
| 0.92 | 0.7414(14) | 0.0172(6) | 0.01415(6) | 0.0139(6) | −0.0093(6) | 0.667(15) | 0.667(6) | 0.668(3) | 2.7259(11) |
| 1.00 | 0.6995(10) | 0.0299(3) | 0.02522(7) | 0.0249(4) | 0.0082(4) | 0.511(10) | 0.510(4) | 0.510(3) | 3.282(12) |
| 1.10 | 0.6361(8) | 0.0533(8) | 0.04522(12) | 0.0440(5) | 0.0345(5) | 0.321(11) | 0.316(5) | 0.318(3) | 4.202(6) |

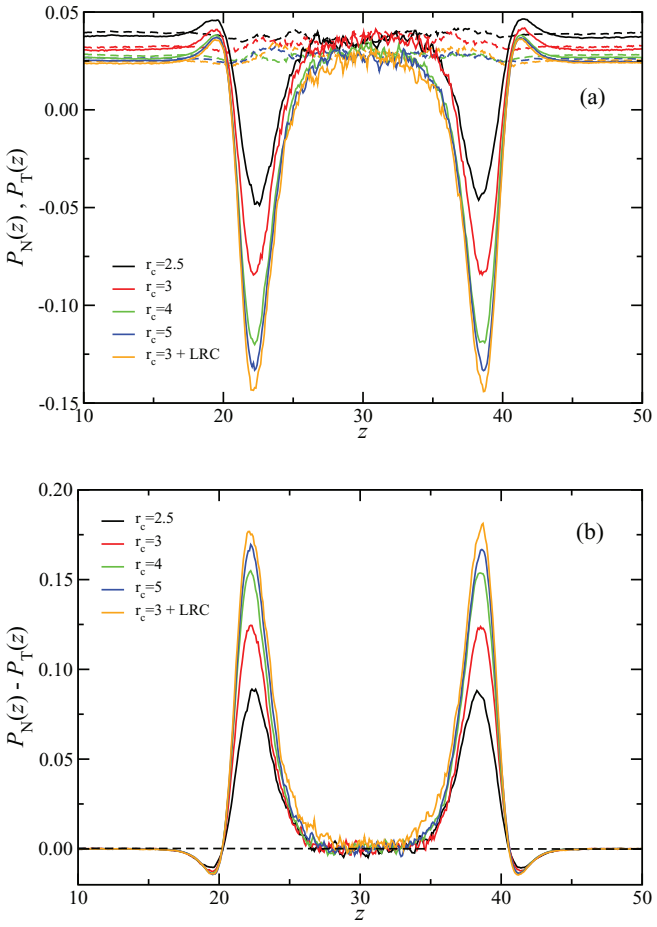


FIG. 2. Normal $P_N(z)$ and tangential $P_T(z)$ (a), and difference between the normal and tangential microscopic components (b) of the pressure tensor profiles across the two vapour-liquid interfaces of spherical LJ molecules at $T = 1.0$. The meaning of the symbols and curves is the same as in Fig. 1.

regions correspond to zones of the interface at which there exist tensions and compressions, as it is explained below. This effect, that can be understood from a microscopic point of view, can be clearly seen in Fig. 2(a). A higher value of the cutoff distance in the intermolecular potential means an increase of the range of the intermolecular forces between particles. As a consequence of this, the zones of the interface at which exist tensions and compressions spread over wider regions of the simulation box, as shown in Fig. 2(a).

As in the case of $P_N(z)$ and $P_T(z)$, the difference between both components of the pressure tensor profiles shows the same qualitative behaviour as at low temperatures. However, the effect of the cutoff distance of the intermolecular potential on $P_N(z) - P_T(z)$ is larger at high temperatures, as can be seen in Figs. 1(b) and 2(b). An interesting feature of the system, shown in Figs. 1 and 2, is that there exist regions at which $P_T(z) < P_N(z)$. Those regions, that correspond to most of the locations at the vapour-liquid interface, are clearly regions of tension. Contrary, small locations of the interface corresponding to zones near the vapour bulk-like regions, are regions of compression in which $P_T(z) > P_N(z)$. The reason for which the transverse pressure has values greater than $P_N$ at the interface near the vapour phase and large negative values (and lower than $P_N$) at other locations of the interface is a consequence of the behaviour of the pressure in the unstable bulk phase region (spinodal region), which plays an essential role in the physics at interfaces. For further details, we recommend the excellent review of Davies and Scriven.[62]

From our knowledge, this is the first time the effect of the cutoff distance and the use of LRC of the dispersive interactions on the structure of $P_N(z)$, $P_T(z)$, and $P_N(z) - P_T(z)$ for the LJ system is analyzed in the same work. The only work, to our knowledge, in which related information has been shown is that of Shen *et al.*[50] These authors show the behaviour of the difference between both components of the pressure tensor of the LJ with $r_c = 2.5$ and 4 in combination with the original method of Janeček[48] at only one temperature, 0.95 (see bottom panel of Fig. 2 of the paper of Shen *et al.*[50]). Note, however, that Janeček[52,53] and co-workers have presented the pressure profiles, at different temperatures, for the LJ system using these LRC.

Once we have analyzed the effect of the cutoff distance on the normal and tangential microscopic components of the pressure tensor profile at two representative temperatures, 0.72 (low) and 1.0 (high), we consider the behaviour of the normal and tangential microscopic components of the pressure tensor profile in the whole range of temperatures at which the system exhibits vapour-liquid phase behaviour, from 0.70 to 1.1. We have used a cutoff distance for the LJ intermolecular potential of $r_c = 3$ with the inhomogeneous LRC described in Sec. II. We have also obtained the normal and tangential macroscopic components of the pressure tensor, $P_N$ and $P_T$, using the VP technique proposed by de Miguel and Jackson,[16] which is based on a thermodynamic definition of the pressure tensor. Since this calculation is only based on energetic considerations, the results are independent of the methodology employed to estimate the contribution to the pressure due to the LRC (Sec. II). The comparison between both results is relevant to this work since it allows to check the validity of the methodology presented in Sec. II to calculate the LRC to the pressure tensor.

The normal and tangential microscopic components of the pressure tensor are presented in Table II. In addition to that, we have averaged the normal microscopic component of the pressure tensor along the vapour phase. As can be seen from Table II, values for the normal macroscopic component of the pressure tensor calculated from the mechanical ($P_N^{vir}$) and thermodynamic ($P_N$) routes are in excellent agreement, confirming that equations proposed in Sec. II predict the correct behaviour of the normal pressure along the whole range of temperatures considered.

Results from the *NVT* calculations in the whole range of temperatures considered are shown in Fig. 3. As can be seen, the $P_N(z)$ and $P_T(z)$ profiles calculated using the IK methodology show the expected behaviour. In particular, the minimum (negative) value of the peaks associated to the tangential microscopic component of the pressure tensor profile, $P_T(z)$, becomes less negative as the temperature is increased. In addition to that, the thickness of the peaks associated to that component increases as the temperature is increased. Since the tangential component contributes positively to the surface

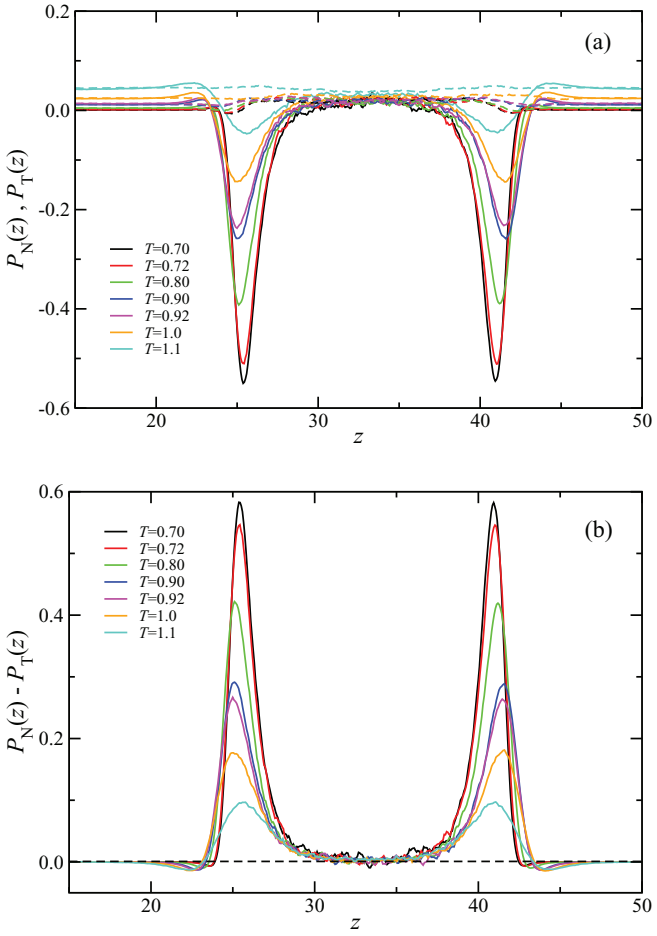


FIG. 3. Normal $P_N(z)$ and tangential $P_T(z)$ (a), and difference between the normal and tangential microscopic components (b) of the pressure tensor profiles across the two vapour-liquid interfaces of spherical LJ molecules using a cutoff distance 3 with inhomogeneous LRC, at temperatures $T = 0.70$ (black), 0.72 (red), 0.80 (green), 0.90 (blue), 0.92 (magenta), 1.0 (orange), and 1.1 (light blue). Continuous and dashed curves in part (a) correspond to the tangential and normal microscopic components of the pressure tensor, respectively.

tension (note that $P_T(z)$ is subtracted from $P_N(z)$ in the mechanical definition of surface tension given by Eq. (1) presented in Sec. I), the behaviour observed in the structure of $P_T(z)$ as the temperature is varied agrees with the expected decrease of the vapour-liquid surface tension with the temperature. The behaviour of the thickness associated to the (negative) peaks exhibited by $P_T(z)$ is similar to that of the interfacial thickness of an interface, that increases with the temperature since it diverges as $T \to T_c$.[1] As shown in Fig. 3(a), regions at which the tangential pressure profile differs from this of the normal pressure increases as the temperature is raised. In order to give a complementary description of the structure of the microscopic components of the pressure tensor profile in the whole range of temperatures at which the system exhibits vapour-liquid phase separation, we have also considered the $P_N(z) - P_T(z)$ profiles, from 0.7 to 1.1, obtained using the full potential. As can be seen in Fig. 3(b), $P_N(z) - P_T(z)$ shows the expected structure, which can be inferred from the results presented in Fig. 3(a).

### B. Effect of the impulsive contribution of the intermolecular force on pressure tensor

The calculation of forces in systems that interact through intermolecular potentials in which interactions are spherically truncated (but not shifted) is cumbersome. Trokhymchuk and Alejandre,[49] and more recently de Miguel and Jackson,[16] have clarified the importance of the additional force due to the discontinuity of the truncated potentials at cutoff distance, which is crucial for inhomogeneous fluids, as it will be shown below, and must be included into the virial if the mechanical route for calculating the pressure is used. The intermolecular force associated to the intermolecular interaction potential $u(r)$ between two LJ molecules separated a distance $r$ is given by $\mathbf{f} = f(r)\hat{\mathbf{r}}$, with $f(r) = -(du/dr)$ and $\hat{\mathbf{r}}$ the unit vector between the interacting molecules. Since in Molecular Dynamics it is common to deal with systems in which forces are spherically truncated (but not shifted), these are usually calculated as

$$f(r) = f_{LJ}(r)\left[1 - \Theta(r - r_c)\right], \tag{14}$$

where $f_{LJ}(r) = -(du_{LJ}/dr)$ is the magnitude of the force associated to the intermolecular LJ potential. As discussed by Trokhymchuk and Alejandre[49] and de Miguel and Jackson,[16] $f(r)$ defined by Eq. (14) does not correspond to the force associated to an intermolecular potential spherically truncated (but not shifted) defined by Eq. (10) (see Sec. III). The right value of the force obtained from Eq. (10) must be calculated as

$$f(r) = f_{LJ}(r)\left[1 - \Theta(r - r_c)\right] + u_c\,\delta(r - r_c), \tag{15}$$

where $u_c = u_{LJ}(r_c)$ is the value of the LJ potential energy at $r = r_c$ and $\delta(x)$ is the $\delta$-Dirac function. The last term on Eq. (15) represents the impulsive (attractive) force, which is by no means negligible. de Miguel and Jackson[16] estimated that the impulsive force accounts for about 6% of the contributions to the total pressure in a bulk LJ liquid phase at $\rho = 0.864$ and $T = 1.5$ when a cutoff distance of $r_c = 2.5$ is used. However, as shown previously by Trokhymchuk and Alejandre,[49] the effect of neglecting the impulsive force has dramatic consequences on the structure of the microscopic components of the pressure tensor profiles. Unfortunately, Trokhymchuk and Alejandre[49] only considered one value of the cutoff distance ($r_c = 2.5$) at one single temperature. Since we are studying the effect of cutoff distance and the use of LRC on the components of pressure tensor, we analyze in detail the structure of the pressure tensor profiles when the impulsive forces are not accounted for.

We now consider the same representative temperatures, 0.72 (low) and 1.0 (high), and study the effect of the cutoff distance on the pressure tensor profiles when the impulsive force at $r = r_c$ is neglected. Values of the normal macroscopic component of the pressure tensor and surface tension obtained from the virial route without the contribution due to the impulsive force, i.e., using Eq. (14), are presented in Table III. Fig. 4(a) shows the $P_N(z)$ and $P_T(z)$ profiles as obtained from *NVT* Monte Carlo simulations using two different cutoff distances, $r_c = 2.5$ and 3 (without LRC and neglecting the impulsive contribution). We have also represented the results calculated including the contribution to the components of the

TABLE III. Normal macroscopic component of the pressure tensor calculated from the virial route, $P_N^{\text{vir}}$, and surface tension calculated from integration given by Eq. (1), $\gamma^{vir}$, for a system of LJ molecules at different temperatures and using two different cutoff distances, $r_c = 2.5$ and 3 (without LRC). Results presented here correspond to simulation data in which forces are calculated using Eq. (14), i.e., the contribution to pressure due to the impulsive force at $r = r_c$ is neglected. All quantities are expressed in the reduced units defined in Sec. III. The errors are estimated as explained in the text. Uncertainties of surface tension calculated from the virial route, $\gamma^{vir}$, are error estimates corresponding to the numerical calculation of the integral given by Eq. (1).

| | $P_N^{vir}$ | | $\gamma^{vir}$ | |
|---|---|---|---|---|
| $T$ | $r_c = 2.5$ | $r_c = 3.0$ | $r_c = 2.5$ | $r_c = 3.0$ |
| 0.70 | 0.00240(3) | 0.00214(7) | 0.679(6) | 0.801(5) |
| 0.72 | 0.00331(2) | 0.00265(12) | 0.633(7) | 0.769(5) |
| 0.80 | 0.00753(2) | 0.00614(23) | 0.503(5) | 0.616(5) |
| 0.90 | 0.02055(12) | 0.0164(3) | 0.341(13) | 0.437(5) |
| 0.92 | 0.02360(8) | 0.0188(3) | 0.319(5) | 0.415(4) |
| 1.00 | 0.04132(10) | 0.0328(3) | 0.197(5) | 0.287(4) |
| 1.10 | 0.07362(2) | 0.0602(6) | 0.081(5) | 0.146(3) |

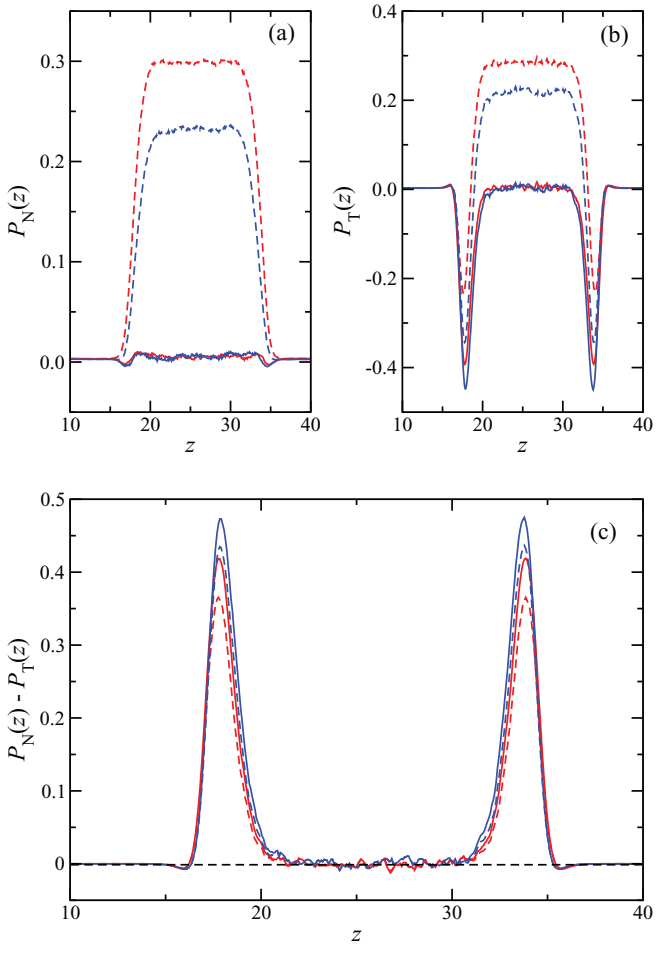


FIG. 4. Normal $P_N(z)$ (a), tangential $P_T(z)$ (b), and difference between the normal and tangential microscopic components (c) of the pressure tensor profiles across the two vapour-liquid interfaces of spherical LJ molecules at $T = 0.72$ and using cutoff distances $r_c = 2.5$ (red) and 3 (blue) without inhomogeneous LRC. Continuous curves correspond to the results obtained using the correct expression for the intermolecular force given by Eq. (15) and dashed curves to the results using the incorrect expression for the intermolecular forces given by Eq. (14).

pressure tensor due to the impulsive force at $r = r_c$. As can be seen in both cases ($r_c = 2.5$ and 3), $P_N(z)$ does not show the correct behaviour along the interface when Eq. (14) is used. The normal pressure profile, as obtained without the impulsive contribution, is approximately correct and constant along the vapour phase. This is expected since the impulsive contribution is negligible at very low densities. Unfortunately, the behaviour of the normal pressure is completely wrong in the liquid region. In particular, the normal pressure is not constant and its value is much higher than the true magnitude. Differences between the correct and wrong values for $P_N(z)$ (along the liquid phase) obtained using $r_c = 2.5$ are larger than those corresponding to the case $r_c = 3$. In particular, the difference between both values varies from 0.3 in the case of $r_c = 2.5$ to 0.23 for $r_c = 3$. This is also an expected result since the impulsive contribution is proportional to the value of the potential energy at $r = r_c^-$, a quantity that decreases as the cutoff distance is increased.

The use of Eq. (14) also introduces important nonphysical effects on the tangential pressure, as can be seen in Fig. 4(b). The characteristic peaks at the interfacial regions are less negative and its behaviour along the liquid slab is completely wrong. Differences between calculations obtained using Eqs. (14) and (15) decrease as the cutoff distance is larger, as previously explained. In particular, the tangential pressure at the liquid phase passes from 0.3 to 0.2 when the cutoff distance increases. Note also that the impulsive contribution is negligible in the vapour phase at this temperature.

Although one of the main goals of this work is to analyze the effect of cutoff distance and LRC on the components of the pressure tensor, it is also interesting to combine the information obtained previously to investigate from this perspective the physical consequences over the interfacial tension. Fig. 4(c) shows the difference between both components of the pressure tensor, $P_N(z) - P_T(z)$, as a function of $z$ for the systems considered, including the use of different cutoff distances and Eqs. (14) and (15). Surprisingly, calculations obtained from Eq. (14) are in qualitative agreement with correct results. Why the structure of $P_N(z) - P_T(z)$ is qualitatively predicted using Eq. (14)? Equations (14) and (15) give similar results since the impulsive contribution is negligible at these densities. Although Eq. (14) provides completely wrong results for $P_T$ and $P_N$ in the liquid phase, the calculations are self-consistent, i.e., $P_N(z) = P_T(z)$ in the bulk regions, including the liquid phase, and hence $P_N(z) - P_T(z) \approx 0$ in this region, giving the correct behaviour in the liquid slab. However, $P_T(z)$ and $P_N(z)$ are not calculated correctly in the interfacial region, and surface tension values obtained using Eq. (14) are only qualitative. In particular, the calculations underestimate the correct width and height of the peaks centered around the two vapour-liquid interfaces.

We have also analyzed the behaviour of both microscopic components of the pressure tensor profile, as well as the difference between both components, at a higher temperature ($T = 1$) using Eqs. (14) and (15). As can be seen in Fig. 5(a), the results at high temperature are similar than those obtained at the low temperature ($T = 0.72$). The normal pressure along the vapour phase, when Eq. (14) is used, is now clearly overestimated. This is a consequence of the increase of density

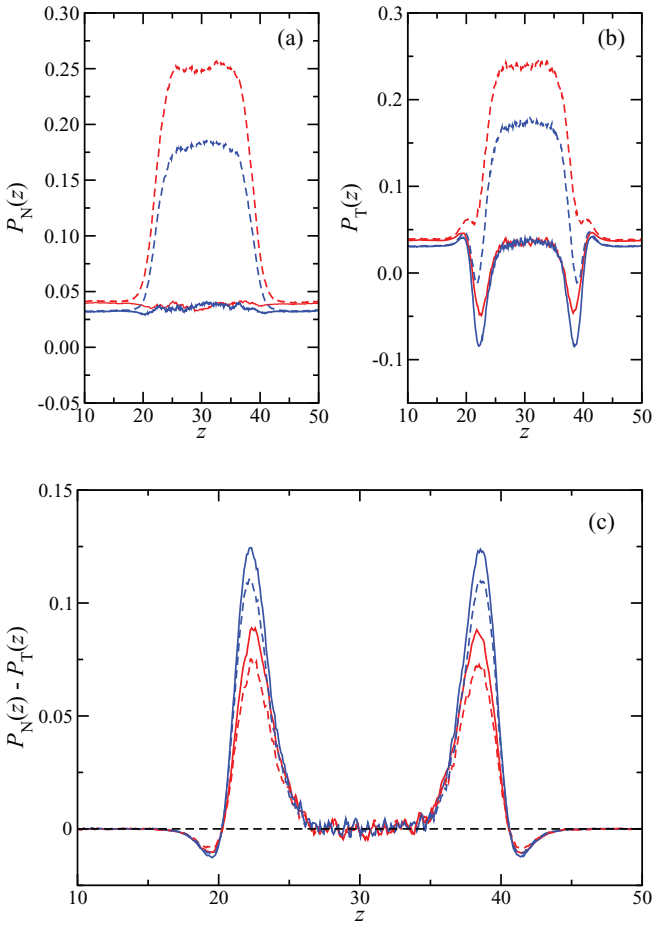


FIG. 5. Normal $P_N(z)$ (a), tangential $P_T(z)$ (b), and difference between the normal and tangential microscopic components (c) of the pressure tensor profiles across the two vapour-liquid interfaces of spherical LJ molecules at $T = 1.00$. The meaning of the symbols and curves is the same as in Fig. 4.

in the vapour phase as the system approaches to the critical point. Note that the contribution to the pressure due to the impulsive force, which is negative (attractive contribution), is proportional to $u_{LJ}(r_c)$ and to the average number of molecular pairs located at distances $r \sim r_c$, or more precisely, between $r_c$ and $r_c + \Delta r$ in the limit $\Delta r \to 0$. The absence of the impulsive contribution produces less attractions, increasing the pressure associated to the truncated force, as shown in Fig. 5(a).

The case of $P_T(z)$ is more complicated although the behaviour is qualitatively similar to that found at $T = 0.72$. As can be seen in Fig. 5(b), differences between $r_c = 2.5$ and 3 are larger than in the previous case (in both cases). Although the shape of $P_T$, as a function of $z$, is similar to that found at lower temperatures for the case $r_c = 3$, the shape of $P_T(z)$ for $r_c = 2.5$ is more complex, including a nonphysical structure at the interfaces due to the use of Eq. (14).

Finally, we have also represented the difference between the components of the pressure tensor, as a function of $z$ (Fig. 5(c)). $P_N(z) - P_T(z)$ exhibits the same behaviour than as low temperature ($T = 0.72$), with the positive peaks lower and wider. The difference between the maximum values of the peaks using Eqs. (14) and (15) are slightly larger than in the previous case ($T = 0.72$), as expected since the temperature considered is closer to the critical temperature of the system.

### C. Density profiles and phase coexistence properties

Once we have analyzed the effect of cutoff distance and LRC on the pressure tensor components, now we turn on the study of other interfacial and thermodynamic properties of the LJ system. Following the same analysis and methodology than in our previous works,[7,19,55–57] we consider different cutoff distances and temperatures. The equilibrium density profiles $\rho(z)$ are computed from averages of the histogram of densities along the $z$ direction over the production stage. The bulk vapour and liquid densities are obtained by averaging $\rho(z)$ over appropriate regions sufficiently removed from the interfacial region. As we have mentioned previously, this procedure is meaningful as far as the central liquid slab is thick enough. This turns out to be the case in our simulations, including those performed at the higher temperatures. The bulk vapour density is obtained after averaging the density profiles on both sides of the liquid film. The statistical uncertainty of these values is estimated from the standard deviation of the mean values. Following our previous works, additional interfacial properties, such as the position of the Gibbs-dividing surface, $z_0$, and the 10–90 interfacial thickness, $t$, are obtained by fitting each of the two equilibrium density profiles to hyperbolic tangent functions[1] (see Eq. (3) of our previous work[19] for further details). We fix liquid, $\rho_L$, and vapour, $\rho_V$, densities to previously computed values and treat $z_0$ and $t$ as adjustable parameters.

Our simulation results for the bulk densities, components of the pressure tensor, surface tension, and interfacial thickness for LJ molecules interacting with the full potential are collected in Tables II and IV, respectively. A detail account for the results obtained for the normal component of the pressure tensor, surface tension, and interfacial thickness for LJ molecules with several cutoff distances has been already presented in Table I.

We show in Fig. 6(a) the density profiles $\rho(z)$ for LJ molecules using different cutoff distances at $T = 0.72$. For the sake of clarity, we only present one half of the profiles corresponding to one of the interfaces. Also for convenience, all density profiles have been shifted along $z$ so as to place $z_0$ at the origin. As can be seen, the slope (in absolute value) of the density profiles in the interfacial region increases as the cutoff distance is increased, making larger the jump in densities when passing from the vapour to the liquid side of the interface. Consequently, the interfacial thickness decreases, an expected result since the cohesive energy of the system is increased, as well as the surface tension, since the cutoff distance is larger. The insets of Fig. 6(a) show the variation of the density profile close to the region of the interface at which the bulk density is reached. As can be seen, relative differences between the density profiles corresponding to a LJ system with $r_c = 2.5$ (without LRC) and $r_c = 3$ (with LRC) are larger close to the vapour phase (∼46%) than to the liquid phase (∼3%).

We have also analyzed the density profile of the system, using the same set of cutoff distances, but now at a higher

TABLE IV. Liquid density, $\rho_L$, vapour density, $\rho_V$, normal macroscopic component of the pressure tensor calculated from the virial route, $P_N^{\rm vir}$, normal and tangential macroscopic components of the pressure tensor calculated from VP, $P_N^{VP}$ and $P_T^{VP}$, respectively, surface tension calculated from integration given by Eq. (1), $\gamma^{vir}$, from VP, $\gamma^{VP}$, and from TA, $\gamma_{TA}$, and 10–90 interfacial thickness, $t$, at different temperatures for systems of LJ molecules with a cutoff distance $r_c = 2.5$ with inhomogeneous LRC. All quantities are expressed in the reduced units defined in Sec. III. The errors are estimated as explained in the text. Uncertainties of surface tension calculated from the virial route, $\gamma^{vir}$, are error estimates corresponding to the numerical calculation of the integral given by Eq. (1).

| $T$ | $\rho_L$ | $\rho_V$ | $P_N^{vir}$ | $P_N^{VP}$ | $P_T^{VP}$ | $\gamma^{vir}$ | $\gamma^{VP}$ | $\gamma_{TA}$ | $t$ |
|---|---|---|---|---|---|---|---|---|---|
| 0.70 | 0.8408(18) | 0.00190(14) | 0.001301(13) | 0.0013(6) | −0.0446(6) | 1.174(14) | 1.161(5) | 1.161(4) | 1.721(3) |
| 0.72 | 0.8328(12) | 0.00255(13) | 0.001781(14) | 0.0015(7) | −0.0419(7) | 1.129(10) | 1.121(5) | 1.119(4) | 1.793(5) |
| 0.80 | 0.7985(12) | 0.0058(5) | 0.00444(5) | 0.0043(7) | −0.0309(7) | 0.946(12) | 0.941(6) | 0.940(3) | 2.098(7) |
| 0.90 | 0.7530(19) | 0.0153(5) | 0.01244(4) | 0.0132(9) | −0.0124(9) | 0.730(10) | 0.721(8) | 0.723(2) | 2.576(14) |
| 0.92 | 0.7434(15) | 0.0162(8) | 0.01328(8) | 0.0142(9) | −0.0096(9) | 0.689(10) | 0.684(8) | 0.685(2) | 2.7101(23) |
| 1.00 | 0.7021(12) | 0.0294(9) | 0.02500(10) | 0.0256(5) | 0.0083(5) | 0.528(14) | 0.524(5) | 0.525(2) | 3.227(16) |
| 1.10 | 0.6417(15) | 0.0534(20) | 0.04543(10) | 0.0454(5) | 0.0357(5) | 0.332(12) | 0.324(5) | 0.3244(19) | 4.326(15) |

temperature, $T = 1$. As can be seen in Fig. 6(b), the same qualitative behaviour is observed, although the change in the slope at the interfacial region seems to be larger. The variation of the profiles close to the region of the interface at which the bulk density is reached exhibits similar increments (in absolute value) than as low temperatures.

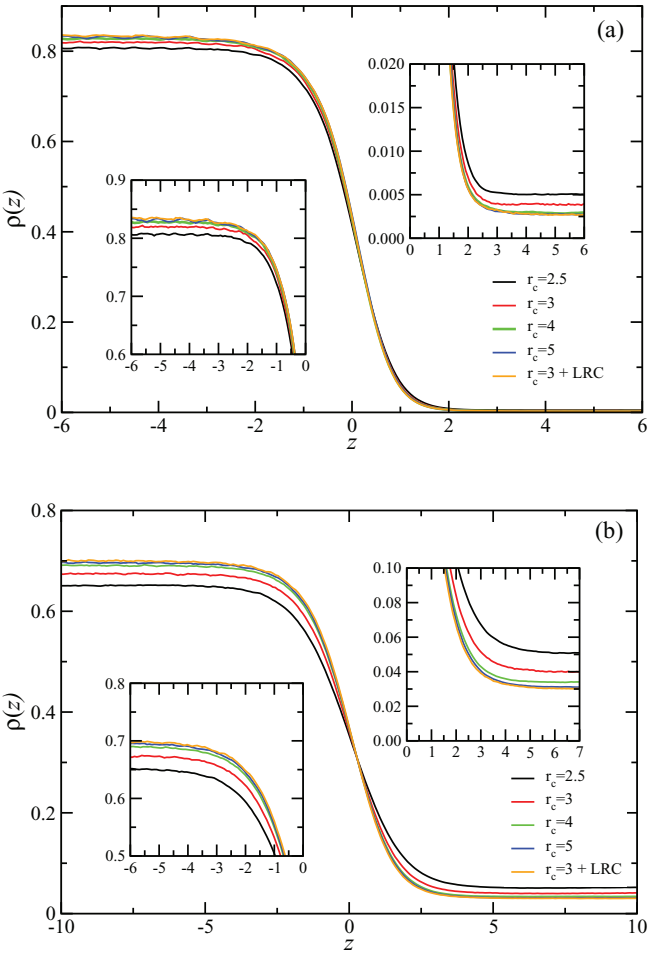


FIG. 6. Simulated equilibrium density profiles across the vapour-liquid interface of spherical LJ molecules using cutoff distances $r_c = 2.5$ (black), 3 (red), 4 (light green), 5 (blue), 2.5 with inhomogeneous LRC (orange), and 3 with inhomogeneous LRC (dark green) at $T = 0.72$ (a) and 1.00 (b). The top and bottom insets in both parts correspond to the near-vapour and near-liquid interfacial region, respectively.

As in our previous works,[7,19,55–57] it is also useful to estimate the location of the critical point resulting from our direct Monte Carlo simulations. The critical temperature $T_c$ and density $\rho_c$ are obtained using the simulation results for the vapour and liquid coexistence densities (Table IV) and the scaling relation for the width of the coexistence curve,

$$\rho_L - \rho_V = A(T - T_c)^{\beta}, \tag{16}$$

and the law of rectilinear diameters

$$\frac{\rho_L + \rho_V}{2} = B + CT. \tag{17}$$

$A$, $B$, and $C$ are constants, and $\beta$ is the corresponding critical exponent. A universal value of $\beta = 0.325$ is assumed here.[1] In Table V, we report the values of the critical temperatures and densities as obtained from this procedure for all the systems studied in this work.

The vapour-liquid density profiles of LJ molecules with a cutoff distance $r_c = 3$ and LRC are depicted in Fig. 7. We have also obtained all the profiles using a slightly lower cutoff distance, $r_c = 2.5$, in combination with the LRC presented in Sec. II. This allows to estimate the effect of the cutoff distance used in determining the interfacial properties of the full intermolecular potential. As seen in Fig. 7, the effect of decreasing the cutoff distance on the density profiles is really very small, especially at low temperatures. Larger differences between profiles calculated using $r_c = 3$ and 2.5 occur at the (vapour and liquid) bulk sides at the highest temperature

TABLE V. Critical temperature and density for LJ molecules with different cutoff distances $r_c$ (and also using LRC) from the analysis of the coexistence densities using Eqs. (16) and (17),[a] and critical temperature obtained from the analysis of the computed surface tension data using Eq. (19) and fixing the critical point to $\mu = 1.258$.[b] All quantities are expressed in the reduced units defined in Sec. III.

| $r_c$ | $\rho_c^{\rm a}$ | $T_c^{\rm a}$ | $T_c^{\rm b}$ |
|---|---|---|---|
| 2.5 | 0.314(9) | 1.190(7) | 1.194(10) |
| 3 | 0.311(10) | 1.234(8) | 1.241(9) |
| 4 | 0.310(10) | 1.271(9) | 1.277(9) |
| 5 | 0.310(14) | 1.283(13) | 1.299(10) |
| 2.5 + LRC | 0.310(12) | 1.305(12) | 1.330(9) |
| 3 + LRC | 0.308(12) | 1.291(11) | 1.322(11) |

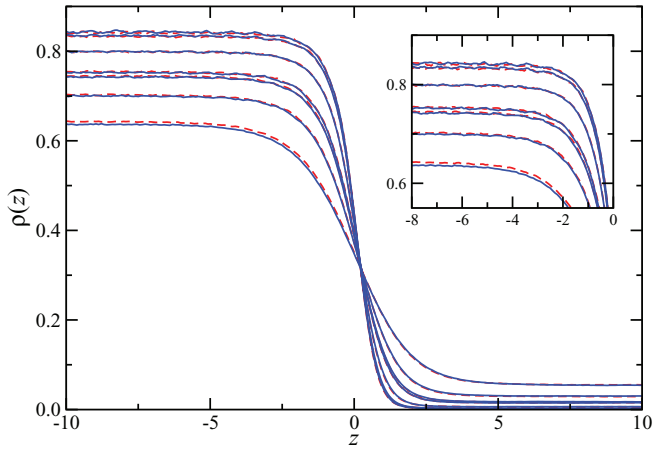


FIG. 7. Simulated equilibrium density profiles across the vapour-liquid interface of spherical LJ molecules using cutoff distances $r_c = 2.5$ (dashed red curves) and 3 (continuous blue curves) with inhomogeneous LRC. From top to bottom (in the liquid region): $T = 0.70$, 0.72, 0.80, 0.90, 0.92, 1.0, and 1.1. Inset corresponds to the enlargement of the liquid region.

($T = 1.1$). Profile obtained using $r_c = 2.5$ predicts a slightly higher liquid density with respect to that obtained using $r_c = 3$ (0.6418(15) and 0.6362(8), respectively) and a lower vapour density (0.0534(7) and 0.0533(3), respectively). In all cases, relative differences are below 1% and within the statistical uncertainties of the simulations (see Tables IV and II for further details).

The vapour-liquid phase envelopes of LJ molecules with $r_c = 2.5$, 3, 4, and 5, and using $r_c = 2.5$ and 3 with inhomogeneous LRC are depicted in Fig. 8. As can be seen, the phase

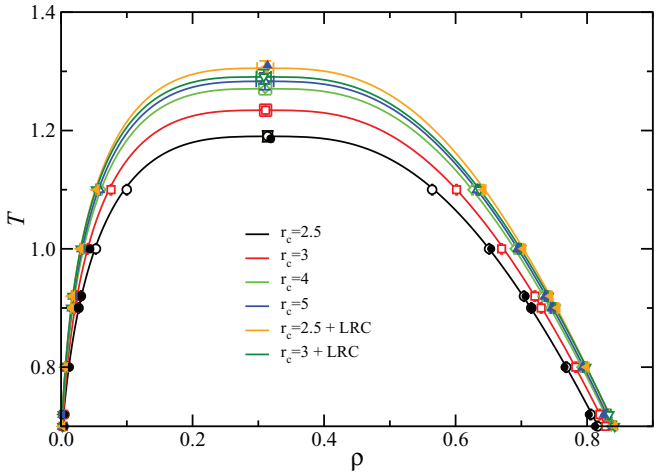


FIG. 8. Vapour-liquid coexistence densities for spherical LJ molecules using different cutoff distances. The open black circles ($r_c = 2.5$), open red squares ($r_c = 3$), open light green diamonds ($r_c = 4$), open blue triangles up ($r_c = 5$), open orange triangles left ($r_c = 2.5$ with inhomogeneous LRC), and open dark green triangles down ($r_c = 3$ with inhomogeneous LRC) correspond to the coexistence densities obtained from MC $NVT$ simulations for spherical molecules with different values of $r_c$. The filled black circles ($r_c = 2.5$) and filled blue triangles up ($r_c = 5.5$) correspond to the coexistence densities obtained by Trokhymchuk and Alejandre,[49] and the filled orange triangles left to those obtained by Janeček.[6] Symbols at the highest temperatures for each of the coexistence curves represent critical points estimated from Eqs. (16) and (17) and those taken from Refs. 6, 49. The curves represent the fits of the simulation data to the scaling relation for the width of the coexistence curve and the law of rectilinear diameters given by Eqs. (16) and (17), respectively.

envelope becomes wider as the cutoff distance is increased. As $r_c$ grows, predictions are closer to the limiting case corresponding to the full potential, which corresponds to the use of a cutoff ($r_c = 2.5$ and 3) with LRC. As in the case of Fig. 6, although results corresponding to calculations performed using $r_c = 2.5$ and 3 with LRC are compatible, simulation data seem to indicate a small dependence of the coexistence liquid density with the cutoff distance. This result indicates that the main approximation of the Janeček's methodology, i.e., the distribution of particles separated beyond $r_c$ is uniform, works slightly better for $r_c = 3$ than $r_c = 2.5$. A possible qualitative explanation of this behaviour may be given taken into account the shape of the radial distribution function at liquid density. This function exhibits a minimum at $r_c = 2.5$ and a maximum at $r_c = 3$. Since the use of LRC implies a uniform particle distribution for $r \geq r_c$, this approximation leads to a more attractive system in the case of $r_c = 2.5$ and a more volatile for $r_c = 3$. This results in lower liquid and higher vapour coexistence densities, as it is observed in Fig. 7.

In order to check the consistency of our results, we have compared the predictions obtained from $NVT$ MC simulations of this work with previous results obtained by several authors using different Monte Carlo and Molecular Dynamics techniques, including grand-canonical transition-matrix Monte Carlo in combination with histogram re-weighting and direct coexistence.[6,35,49,50] As can be seen in Fig. 8, results obtained in this work are in excellent agreement with all the data taken from the literature in all cases. In addition to that, Fig. 8 also shows a good agreement between critical temperatures and densities obtained here and those taken from the literature. Critical data obtained from simulation in this work from vapour-liquid coexistence data and surface tension analysis are presented in Table V.

Since the vapour pressure of the system is equal to the normal component of the pressure tensor, we have represented the vapour pressure, as a function of temperature, in Fig. 9. In particular, we have analyzed the effect of the cutoff distance on the vapour pressure. In addition to that, we have included the data corresponding to the $r_c = 2.5$ and 3 with LRC. We have also compared our results with simulation data taken from the work of Trokhymchuk and Alejandre[49] for several cutoff distances. As can be seen, the main effect of increasing the cutoff distance is to decrease the vapour pressure of the system. This is the expected behaviour since as the cutoff distance increases, more attractions are account for in the system, and the vapour pressure decreases. Agreement between results obtained in this work and simulation data taken from the literature is excellent in all cases.

### D. Interfacial thickness

Another interesting property obtained from our analysis is the 10–90 interfacial thickness (cf. Tables IV, II, and I). For a given cutoff distance, $t$ is seen to increase with temperature, which simply reflects the fact that the interfacial region gets correspondingly wider, in agreement with our previous results, as can be observed in Fig. 10. At low temperatures, the density profiles exhibit a sharp interface, which corresponds

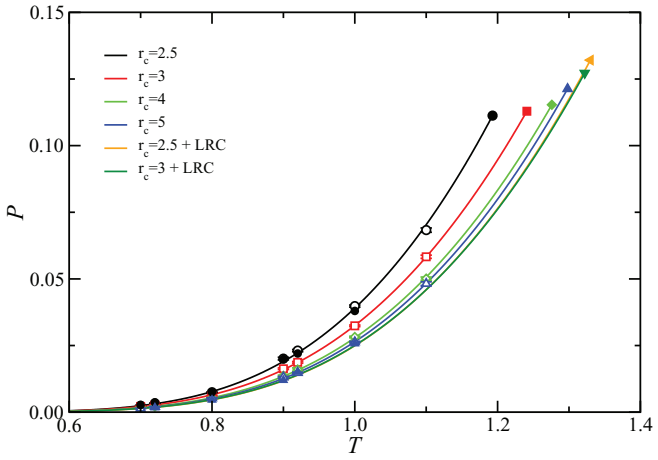


FIG. 9. Vapour pressure, as a function of temperature, for spherical LJ molecules using different cutoff distances. The open symbols correspond to the normal microscopic component of the pressure tensor averaged along the vapour phase (taken from Tables IV, II, and I) obtained from MC $NVT$ simulations for spherical molecules with different values of $r_c$. The meaning of the symbols are the same as in Fig. 8. The continuous curves correspond to Clausius-Clapeyron equation fitted to the vapour pressure data. Symbols at the highest temperatures for each of the vapour pressure curves represent critical points estimated from Eqs. (16) and (17) (critical temperatures) and the Clausius-Clapeyron equation (critical pressures).

to a low value of the interfacial thickness. As the temperature is increased towards the critical value, the interfacial region becomes wider, and hence, the value of the interfacial thickness increases and diverges to infinity as $T \to T_c$. The variation of interfacial thickness with temperature for different cutoff distances is illustrated in Fig. 10. We have also included the results corresponding to the full potential. We have compared our predictions with MC simulation results obtained by Janeček[6] using LRC. As can be seen, agreement between both results is excellent in the whole range of temperatures studied. According to the figure, increasing the cutoff distance results in a decrease of the thickness of the interface at fixed temperature, which is consistent with the fact that the systems with larger cutoff distances have a larger cohesive energy. This behaviour is consistent with that found for the shape of the vapour-liquid phase envelopes.

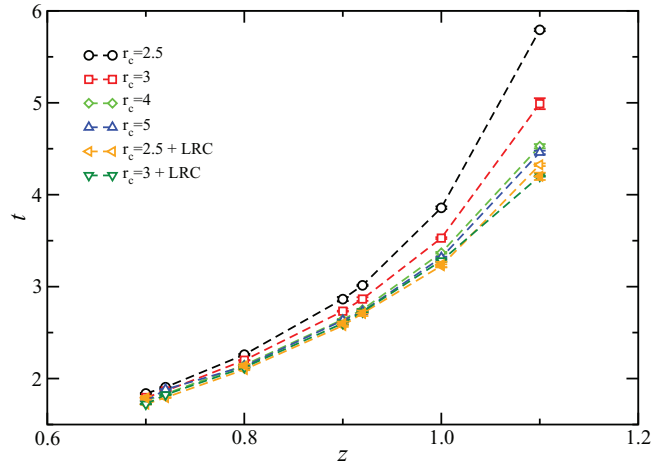


FIG. 10. The 10–90 interfacial thickness as a function of the temperature for spherical LJ molecules using different cutoff distances. The meaning of the open symbols are the same as in Fig. 8. The filled orange triangles left correspond to the interfacial thickness obtained MC $NVT$ simulations of spherical LJ molecules with $r_c = 2.5$ with inhomogeneous LRC obtained by Janeček.[6] The curves are included as a guide to eyes.

### E. Surface tension

Finally, we have calculated the vapour-liquid surface tension of LJ molecules using several cutoff distances without LRC, as well as using the full potential. In particular, we have determined the surface tension using its mechanical definition that involves the integration of the difference between the tangential and normal microscopic components of the pressure tensor profiles, as obtained from the IK methodology, along the simulation box according to Eq. (1). In addition to that, we have also determined the surface tension using two perturbative approaches: the TA method of Gloor *et al.*[3] and the VP technique of de Miguel and Jackson.[16] In first case, the surface tension is determined performing virtual area perturbations of a (small) magnitude during the course of the simulation at constant volume. In the second case, the surface tension is determined in two steps. In the first step, the normal and tangential macroscopic components of the pressure tensor, $P_N$ and $P_T$, are calculated from their thermodynamic definitions as proposed by de Miguel and Jackson.[16] In the second step, the surface tension $\gamma$ is obtained from the relationship (see Eq. (21) of the work of de Miguel and Jackson[16]),

$$\gamma = L_Z(P_N - P_T). \tag{18}$$

Here, $L_z$ is the simulation length along the z-axis. Note that Eq. (18) can be viewed as the macroscopic version of Eq. (1). As in the case of the microscopic definition, since there exist two vapour-liquid interfaces, the true value associated to a single interface is half of the value obtained from Eq. (18).

The calculation of the surface tension through three different but complementary routes allows to compare the results obtained from the mechanical and thermodynamic methods. This is another convincing test for consistency for the inhomogeneous LRC presented in Sec. II. Note that similar consistent results have been found in previous applications of the method for calculating the total potential energy of the system.[7,55–57]

The temperature dependence of the surface tension for LJ molecules using different cutoff distances is shown in Fig. 11. We have also included the results corresponding to the full potential. The results are also compared with simulation data taken from the literature for the LJ system with different cutoff distances and using the original Janeček's methodology.[6,35,49,50] Agreement between our simulations and data taken from the literature are in excellent agreement in all cases, demonstrating that the methodology proposed in Sec. II is consistent with the original formulation of Janeček.[6] As can be seen, at any given temperature, the interfacial tension is larger for molecules with larger cutoff distance. Once again, this is consistent with the larger cohesive energy in systems consisting of molecules in which attractive interactions are longer. As can be seen from Fig. 11, a nearly linear behaviour is found for the range of temperatures considered

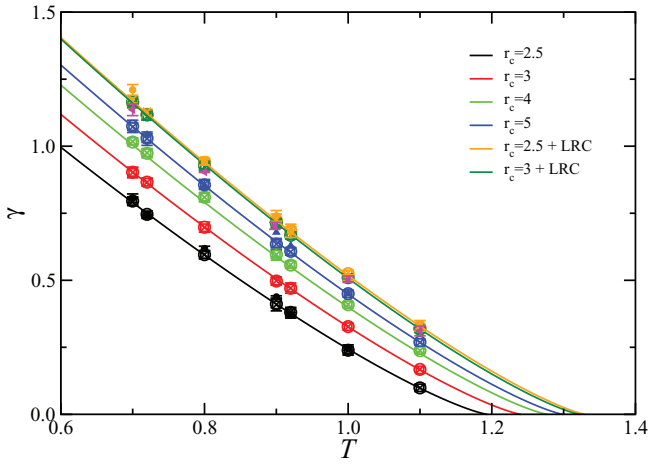


FIG. 11. Surface tension as a function of the temperature for spherical LJ molecules using cutoff distances $r_c = 2.5$ (black), 3 (red), 4 (light green), 5 (blue), 2.5 with inhomogeneous LRC (orange), and 3 with inhomogeneous LRC (dark green). Different symbols represent the surface tension obtained from MC $NVT$ simulations for spherical molecules using the mechanical route of Irving and Kirkwood[8] (open circles), the VP method of de Miguel and Jackson[16] (open squares), and the TA technique[3] (crosses). The filled black circles ($r_c = 2.5$) and filled blue triangles up ($r_c = 5.5$) correspond to the surface tension obtained by Trokhymchuk and Alejandre[49] using the mechanical route, the filled orange circles to the MC simulation data by Janeček,[6] and the filled magenta left triangles to those obtained by Shen *et al.*[50] The curves represent the fits of the simulation data to the scaling relationship of the surface tension near the critical point given by Eq. (19) with $\mu = 1.258$.

here, with a slight curvature close to the critical point for each system.

A comparison between the surface tension values obtained using $r_c = 2.5$ and 3 in combination with LRC reveals a tiny dependence with the value of the cutoff distance used. Although differences between both results are really small (see Tables II and IV for comparison), deviations seem to be systematic and larger than the estimated errors, especially at temperatures $T \gtrsim 0.90$, indicating that the main approximation of the Janeček's[6] method works slightly better for the case $r_c = 3$.

The computed values of the surface tension allow us to obtain an independent estimate of the critical temperature for each cutoff used from the scaling relation

$$\gamma = \gamma_0 \left(1 - T/T_c\right)^{\mu}, \tag{19}$$

where $\gamma$ is the surface tension at temperature $T$, $\gamma_0$ is the "zero-temperature" surface tension, $\mu$ is the corresponding critical exponent, and $T_c$ is the critical temperature. Here, we fix $\mu$ to the universal value of $\mu = 1.258$ as obtained from renormalization-group theory.[1] Our estimates for the critical temperatures are collected in Table V. The overall agreement between these values and those obtained from an analysis of the coexistence densities is satisfactory.

## V. CONCLUSION

We have proposed an improved version of the Janeček[6] methodology to evaluate the contribution to the microscopic components of the pressure tensor due to the dispersive inhomogeneous LRC of spherical LJ fluid. This improved technique allows to determine the contribution as an effective pairwise virial, without need of the explicit calculation of the current density profile along the simulation. In order to assess the accuracy of the method proposed, we have determined the interfacial properties of the vapour-liquid interface of spherical LJ molecules with different spherically truncated (but not shifted) distances, $r_c = 2.5$, 3, 4, and $5\sigma$. In addition to that, we have also obtained the same properties using cutoff distances $r_c = 2.5$ and $3\sigma$ in combination with the improved version of the inhomogeneous LRC of Janeček[6] proposed in this work.

We use Monte Carlo $NVT$ simulations of the inhomogeneous system containing two vapour-liquid interfaces. The normal and tangential microscopic components of the pressure tensor are evaluated using the mechanical or virial route in combination with the recipe of Irving and Kirkwood.[8] We have also determined the macroscopic components of the pressure tensor using the alternative VP method of de Miguel and Jackson.[16] In addition to that, the vapour-liquid surface tension has been evaluated using three different but equivalent procedures, the integration of the difference between the microscopic components of the pressure tensor following the mechanical route, the difference of the macroscopic components obtained from the thermodynamic perturbative method, and finally the well-known TA approach. We have examined the density profiles, interfacial thickness, and surface tension in terms of the temperature and the cutoff distance of the intermolecular potential. In addition, we have also calculated the coexistence phase envelope, including the location of the critical point from an analysis of the density profiles and the surface tension, and the vapour pressure. Results obtained in this work are in excellent agreement with simulation data taken from literature in all cases, confirming the adequacy of the methodology for calculating the inhomogeneous LRC.

The effect of the cutoff distance $r_c$ on the microscopic and macroscopic components of the pressure tensor, surface tension, density profiles, and interfacial thickness, as well as other thermodynamic properties associated to the vapour-liquid equilibrium, such as the coexistence densities, vapour pressure, and critical temperature and density has been investigated. The normal macroscopic and microscopic components of the pressure tensor decrease and the peak of the microscopic component of the pressure tensor associated to the interface becomes more negative as the cutoff distance is increased, approaching to the full potential limit when the inhomogeneous LRC for the intermolecular potential and virial are used. The vapour-liquid interface is seen to sharpen with increasing the cutoff distance corresponding to an increase in the width of the coexistence phase envelope, and an accompanying increase in the surface tension. This is a direct consequence of the cohesive energy of the system, that increases when larger cutoff distances or inhomogeneous LRC are used.

Finally, we have also checked the effect of the impulsive contribution to the pressure due to the discontinuity of the intermolecular interaction potential when is cut (but not shifted) at $r_c$. If this contribution is not accounted for in the calculation of the microscopic components of the pressure tensor, incorrect values of both components as well as a wrong structure

along the vapour-liquid interface are obtained. This effect is more important for short cutoff distances, an expected result since the jump at $r_c$ is larger.

## ACKNOWLEDGMENTS

The authors would like to acknowledge helpful discussions with J. M. Míguez, L. G. MacDowell, and M. M. Piñeiro. This work was supported by Ministerio de Ciencia e Innovación (MICINN, Spain) (Grant No. FIS2010-14866) and by Ministerio de Economía y Competitividad (MINECO) (Grant No. FIS2013-46920-C2-1-P). Further financial support from Junta de Andalucía and Universidad de Huelva is also acknowledged.

[1]J. S. Rowlinson and B. Widom, *Molecular Theory of Capillarity* (Clarendon Press, 1982).
[2]F. Varnik, J. Baschnagel, and K. Binder, J. Chem. Phys. **113**, 4444 (2000).
[3]G. J. Gloor, G. Jackson, F. J. Blas, and E. de Miguel, J. Chem. Phys. **123**, 134703 (2005).
[4]L. G. MacDowell, J. Benet, and N. A. Katcho, Phys. Rev. Lett. **111**, 047802 (2013).
[5]L. G. MacDowell, J. Benet, N. A. Katcho, and J. M. Palanco, Adv. Colloid Interface Sci. **206**, 150 (2014).
[6]J. Janeček, J. Phys. Chem. B **110**, 6264–6269 (2006).
[7]L. G. MacDowell and F. J. Blas, J. Chem. Phys. **131**, 074705 (2009).
[8]J. H. Irving and J. G. Kirkwood, J. Chem. Phys. **18**, 817 (1950).
[9]A. Harasima, Adv. Chem. Phys. **1**, 203 (1958).
[10]J. Alejandre and G. A. Chapela, J. Chem. Phys. **132**, 014701 (2010).
[11]G. A. Chapela and J. Alejandre, J. Chem. Phys. **135**, 084126 (2011).
[12]G. A. Chapela, E. Día-Herrera, J. C. Armas-Pérez, and J. Quintana-H, J. Chem. Phys. **138**, 224509 (2013).
[13]J. C. Armas-Pérez, J. Quintana, and G. A. Chapela, J. Chem. Phys. **139**, 024505 (2013).
[14]J. C. Neyt, A. Wender, V. Lachet, and P. Malfreyt, J. Phys. Chem. C **116**, 10563 (2012).
[15]J. C. Neyt, A. Wender, V. Lachet, A. Ghoufi, and P. Malfreyt, J. Chem. Phys. **139**, 024701 (2013).
[16]E. de Miguel and G. Jackson, J. Chem. Phys. **125**, 164109 (2006)
[17]E. de Miguel and G. Jackson, Mol. Phys. **104**, 3717 (2006).
[18]P. E. Brumby, A. J. Haslam, E. de Miguel, and G. Jackson, Mol. Phys. **109**, 169 (2010).
[19]F. J. Blas, L. G. MacDowell, E. de Miguel, and G. Jackson, J. Chem. Phys. **129**, 144703 (2008).
[20]G. Galliero, J. Chem. Phys. **133**, 074705 (2010).
[21]A. Ghoufi and P. Malfreyt, Mol. Simul. **39**, 603 (2013).
[22]C. Vega and E. de Miguel, J. Chem. Phys. **126**, 154707 (2007).
[23]J. M. Míguez, D. González-Salgado, J. L. Legido, and M. M. Piñeiro, J. Chem. Phys. **132**, 184102 (2010).
[24]G. Galliero, M. M. Piñeiro, B. Mendiboure, C. Miqueu, T. Lafitte, and D. Bessières, J. Chem. Phys. **130**, 104704 (2009).
[25]E. de Miguel, N. G. Almarza, and G. Jackson, J. Chem. Phys. **127**, 034707 (2007).
[26]C. Miqueu, J. M. Míguez, M. M. Piñeiro, T. Lafitte, and B. Mendiboure, J. Phys. Chem. B **115**, 9618 (2011).
[27]F. Biscay, A. Ghoufi, V. Lachet, and P. Malfreyt, J. Chem. Phys. **131**, 124707 (2009).
[28]A. Ghoufi, F. Goujon, V. Lachet, and P. Malfreyt, J. Chem. Phys. **128**, 154716 (2008).
[29]A. Ghoufi, F. Goujon, V. Lachet, and P. Malfreyt, Phys. Rev. E **77**, 031601 (2008).
[30]F. Biscay, A. Ghoufi, F. Goujon, and P. Malfreyt, J. Phys. Chem. B **112**, 13885 (2008).
[31]F. Biscay, A. Ghoufi, F. Goujon, V. Lachet, and P. Malfreyt, J. Chem. Phys. **130**, 184710 (2009).
[32]F. Biscay, A. Ghoufi, V. Lachet, and P. Malfreyt, Phys. Chem. Chem. Phys. **11**, 6132 (2009).
[33]J. C. Neyt, A. Wender, V. Lachet, A. Ghoufi, and P. Malfreyt, J. Chem. Theory Comput. **10**, 1887 (2014).
[34]A. P. Lyuvartsev, A. A. Martsinovski, S. V. Shevkunov, and P. N. Vorontsov-Velyaminov, J. Chem. Phys. **96**, 1776 (1992)
[35]J. R. Errington and D. A. Kofke, J. Chem. Phys. **127**, 174709 (2007).
[36]E. de Miguel, J. Phys. Chem. B **112**, 4674 (2008).
[37]L. G. MacDowell and P. Bryk, Phys. Rev. E **75**, 061609 (2007).
[38]J. Benet, L. G. MacDowell, and C. Menduiña, J. Chem. Eng. Data **55**, 5465 (2010).
[39]R. de Gregorio, J. Benet, N. A. Katcho, F. J. Blas, and L. G. MacDowell, J. Chem. Phys. **136**, 104703 (2012).
[40]F. J. Martínez-Ruiz, F. J. Blas, L. G. MacDowell, and A. I. Moreno-Ventas Bravo, "Vapor-liquid interfacial properties of square-well chains" (unpublished).
[41]M. P. Allen, *Computer Simulation of Liquids* (Clarendon, Oxford, 1987).
[42]D. Frenkel and B. Smit, *Understanding Molecular Simulations*, 2nd ed. (Academic, San Diego, 2002).
[43]E. M. Blokhius, D. Bedeaux, C. D. Holcomb, and J. A. Zollweg, Mol. Phys. **15**, 665 (1995).
[44]M. Mecke, J. Winkelmann, and J. Fischer, J. Chem. Phys. **107**, 9264 (1997).
[45]M. Mecke, J. Winkelmann, and J. Fischer, J. Chem. Phys. **110**, 1188–1194 (1999).
[46]K. C. Daoulas, V. A. Harmandaris, and V. G. Mavrantzas, Macromolecules **38**, 5780 (2005).
[47]M. Guo and B. C.-Y. Lu, J. Chem. Phys. **106**, 3688–3695 (1997).
[48]J. Janeček, H. Krienke, and G. Schmeer, J. Phys. Chem. B **110**, 6916–6923 (2006).
[49]A. Trokhymchuk and J. Alejandre, J. Chem. Phys. **111**, 8510 (1999).
[50]V. K. Shen, R. D. Mountain, and J. R. Errington, J. Phys. Chem. B **111**, 6198–6207 (2007).
[51]G. A. Chapela, G. Saville, S. M. Thompson, and J. S. Rowlinson, J. Chem. Soc. Faraday Trans. **73**, 1133–1144 (1977).
[52]J. Janeček, H. Krienki, and G. Schmeer, Condens. Matter Phys. **10**, 415 (2007).
[53]J. Janeček, J. Chem. Phys. **131**, 124513 (2009).
[54]See supplementary material at http://dx.doi.org/10.1063/1.4900773 for long-range corrections for the pressure tensor of spherical systems.
[55]F. J. Blas, F. J. Martínez-Ruiz, A. I. Moreno-Ventas Bravo, and L. G. MacDowell, J. Chem. Phys. **137**, 024702 (2012).
[56]F. J. Blas, A. I. Moreno-Ventas Bravo, J. M. Míguez, M. M. Piñeiro, and L. G. MacDowell, J. Chem. Phys. **137**, 084706 (2012).
[57]F. J. Blas, A. I. Moreno-Ventas Bravo, J. Algaba, F. J. Martínez-Ruiz, and L. G. MacDowell, J. Chem. Phys. **140**, 114705 (2014).
[58]J. M. Míguez, M. M. Piñeiro, and F. J. Blas, J. Chem. Phys. **138**, 034707 (2013).
[59]F. J. Blas and B. Mendiboure, J. Chem. Phys. **138**, 134701 (2013).
[60]R. Eppenga and D. Frenkel, Mol. Phys. **52**, 1303 (1984).
[61]V. I. Harismiadis, J. Vorholz, and A. Z. Panagiotopoulos, J. Chem. Phys. **105**, 8469 (1996).
[62]H. T. Davies and L. E. Scriven, Adv. Chem. Phys. **49**, 357 (1982).